THE JOURNAL OF THE ALABAMA ACADEMY OF SCIENCE

Volume 92 **November 2021** **No. 2**

Cover Photograph: AI generated rat photo using the phrase “a photo of a rat walking through grass” using DALL-E. Artistic photograph credit: Brian Toone.

Editorial Comment:
On behalf of the Alabama Academy of Science, I would like to express my gratitude and appreciation to the reviewers for their valuable contributions in reviewing the manuscripts of this issue.

Thanks!
Brian Toone
Editor: Alabama Academy of Science Journal

**THE JOURNAL OF THE
ALABAMA ACADEMY OF SCIENCE
AFFILIATED WITH THE
AMERICAN ASSOCIATION FOR THE
ADVANCEMENT OF SCIENCE**

VOLUME 92 NOVEMBER 2021 NO. 2

Publication and Subscription Policies:
Submit all manuscripts and pertinent correspondence to the Editor. Each manuscript will receive at least two simultaneous reviews. For style details, follow instructions to Authors available on the Alabama Academy of Science website – http://alabamaacademyofscience.org

Reprints requests must be addressed to the editor: brtoone@samford.edu

Subscriptions and Journal Exchanges: Address all Correspondence to the Chairman of the Editorial Board.

ISSN 002-4112

TABLE OF CONTENTS

ARTICLES

SEX DIFFERENCES IN EFFECTS OF ILEAL INTERPOSITION SURGERY ON GLUCOSE REGULATION IN MELANOCORTIN-4 RECEPTOR DEFICIENT RATS.
Ping Zhao (pzhao1@una.edu), Alicia Kiechler, Elliott Zieman, Meet Maheshbhai Patel, Kai Xue and April D. Strader **57**

AN EXAMINATION OF THE SUNSPOT AREAL DATASET, 1875–2017: PAPER II, HEMISPHERIC DIFFERENCES
Robert Wilson, NASA Marshall Space Flight Center, NSSTC, Huntsville, AL (robert.m.wilson@nasa.gov) **69**

EXTRA

Minutes of the Executive Committee Meeting, October 2021.....92

SEX DIFFERENCES IN EFFECTS OF ILEAL INTERPOSITION SURGERY ON GLUCOSE REGULATION IN MELANOCORTIN-4 RECEPTOR DEFICIENT RATS.

Ping Zhao[1,2], Alicia Kiechler[1], Elliott Zieman[3], Meet Maheshbhai Patel[2], Kai Xue[4] and April D. Strader[1]

[1]Department of Physiology, Southern Illinois University School of Medicine, Carbondale, Illinois 62901; [2]Department of Biology, University of North Alabama, Florence, AL 35632; [3]Department of Biological Science, Eastern Illinois University, Charleston, IL 61920; [4]State Key Laboratory of Medical Genomics, Ruijin Hospital Affiliated to Shanghai Jiao Tong University School of Medicine, Shanghai, China

Correspondence: Ping Zhao (pzhao1@una.edu)

ABSTRACT

We aimed to determine the metabolic differences between male and female rats after ileal interposition surgery and determine whether the remission of insulin resistance after ileal interposition is dependent on melanocortin-4 receptor signaling in both male and female rats. All age-matched male and female rats were treated with either sham or ileal interposition surgery. Glucose tolerance tests and body composition analysis were then performed. Our results indicated a loss of *Mc4r* function in both male and female rats induced obesity; male knockout rats with sham surgery, not female knockout rats with sham surgery, showed impaired glucose tolerance; insulin resistance of both knockout sham rats and pairfeeding sham rats is significantly higher than that of knockout interposition rats and pairfeeding interposition rats respectively in both male and female rats; interposition surgery decreased both fat percentage and fat mass in female rats, not in male rats, in the long run. In conclusion, Melanocortin-4 Receptor signaling is not necessary for the underlying beneficial effects of ileal interposition on glucose metabolism and insulin resistance. Female rats might get more stable benefits than male rats after the surgery.

INTRODUCTION

Melanocortin-4 receptor (MC4R) in the brain plays a critical role in regulating energy homeostasis [1-3]. *MC4R* gene mutations have a prevalence of 1-2.5% in people with BMI of greater than 30 and are the most frequent monogenic cause of early-onset human obesity and insulin resistance [4-7]. Obesity surgery (bariatric surgery) has been the most effective way to reduce body weight [8]. One notable and particularly interesting effect is the rapid and durable remission of insulin resistance after bariatric surgery, an effect independent of body weight loss [9]. However, it is unclear whether bariatric surgery can resolve insulin resistance caused by complete *MC4R* gene mutation in obese patients due to the limited number of the patients with this condition [10, 11]. One study about Roux-en-Y gastric bypass (RYGB) surgery, the most commonly performed bariatric procedure in the United States, in *Mc4r*-deficient mice has found that the mice do not benefit from the surgery to the same degree as *Mc4r*-heterozygous mice,

thus suggesting that *Mc4r* is required for improved glucose or insulin sensitivity [12]. However, another study of vertical sleeve gastrectomy (VSG), a different type of bariatric procedure, in *Mc4r*-deficient rats has found that VSG improves glucose metabolism in these rats, thus indicating that remission of insulin resistance is not mediated by alterations in *Mc4r* activity [13]. Both RYGB and VSG cause body weight loss that might influence the level of insulin resistance and consequently lead to conflicting results. Therefore, our study chose ileal interposition (IT) surgery (which does not result in weight loss) in *Mc4r*-deficient rats to determine whether *Mc4r* signaling is required to increase insulin sensitivity after bariatric surgery.

Ileal interposition surgery mainly improves insulin sensitivity without significant body weight loss[14, 15], which provides insight into the effectiveness of bariatric surgery [16]. Additionally, most studies use only male rats and little is known about the sexual differences between males and females after the surgeries. The sexual difference is very important because approximately 85% of the patients who have received bariatric surgery are female [17]. Therefore, we performed IT surgery in both male and female rats with *Mc4r* deficiency to determine whether the *Mc4r* signaling is necessary in resolving insulin resistance and identify the sex-specific differences after IT surgery.

METHODS

Animals

Fifty-four age-matched rats (male, n = 25; female, n = 29) were the 7th littermates from rats with a *Mc4r* heterozygous mutation (Transposagen's *Mc4r* TGEM® Rat Model from Transposagen Biopharmaceuticals, Lexington, KY, USA), an ENU-induced point mutation (K314X) that introduces a premature stop codon in the 8th helix of *Mc4r* [18]. DNA isolation and genotyping of experimental rats were performed as previously described [19]. In brief, DNA was processed from ear punches and genotyped to detect the ENU-induced single nucleotide polymorphism (SNP) in *Mc4r* (K314X) by using the KASPar SNP genotyping system (KBiosciences; Hoddesdon, UK). All experimental rats were weaned at postnatal day (PND) 21, group-housed (2/cage) until postnatal day (PND) 42, and subsequently housed individually. Rats were maintained on a 12:12-h light-dark cycle. All rats were given ad libitum access to water and a pelleted low-fat chow diet. All animal procedures and blood collection were approved by the Institutional Animal Care and Use Committee of Southern Illinois University-Carbondale; all experiments and methods in the study were performed in accordance with the guidelines and regulations approved by the Office of Sponsored Projects Administration of Southern Illinois University.

Surgery and Experimental Design

On postnatal day (PND) 56, all fifty-four rats received either sham or IT surgery by the same group of surgeons and were divided into twelve groups in total (Figure 1. Illustration of experimental design). The six male groups included four wild type rats treated with sham surgery (WT Sham); five WT rats treated with IT surgery (WT IT); four *Mc4r* knockout rats treated with sham surgery (KO Sham); four KO rats treated with IT surgery (KO IT); four KO rats treated with sham surgery and pair feeding (PF Sham); four KO rats treated with IT and pair feeding (PF IT). The six female groups included four wild type rats treated with sham surgery (WT Sham); five WT rats treated with IT surgery (WT IT); five *Mc4r* Knock-out rats treated with sham surgery (KO Sham); five KO rats treated with IT surgery (KO IT); five KO rats treated with

sham surgery and pair feeding (PF Sham); five KO rats treated with IT and pair feeding (PF IT). Body weight was measured daily until postoperative day (POD) 14 and then were monitored weekly until POD 161. On POD 28, an oral glucose tolerance test (OGTT) was completed and an EchoMRI was performed on both POD 30 and POD 161. The pair feeding ended on POD 35 and the rats were sacrificed on POD 161 after the second EchoMRI.

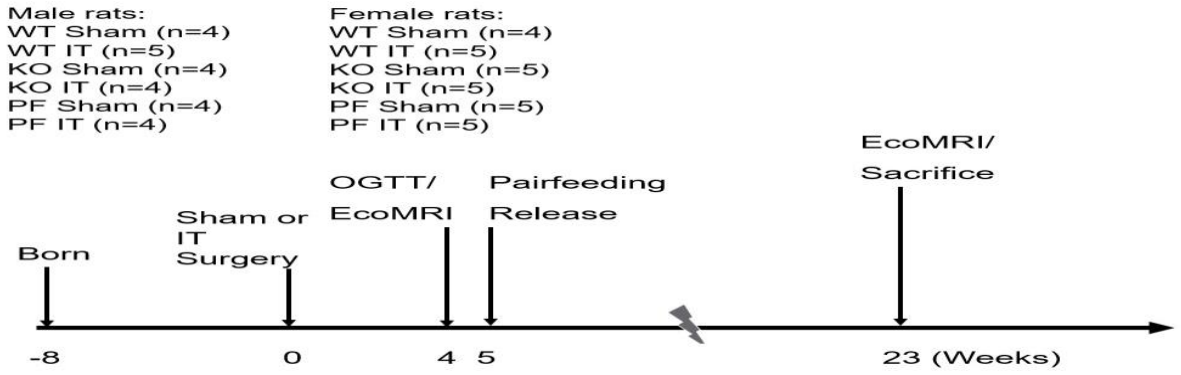

Figure 1. Illustration of experimental design.

Ileal Interposition Surgery

Rats were treated with either sham or ileal interposition (IT) as previously described [15]. Rats were anesthetized with isoflurane anesthesia (2%) during the procedure. Briefly, a midline abdominal incision was made and the caecum was externalized. Intestinal transections were made at 5 and 15 cm proximal to the ileocecal valve to isolate a 10-cm segment of ileum. A single anastomosis was made using a 7-0 silk suture (Ethicon, Cincinnati, OH, USA) at the site of the segment removal. The segment was laid aside and kept moist with warmed 0.9% saline while the remaining intestines were externalized to locate the ligament of Treitz. The jejunum was transected 5 cm distal to the ligament of Treitz and the segment was interposed using an anastomosis in an iso-peristaltic direction. The intestines were bathed in 0.9% saline and re-inserted into the abdominal cavity. Sham-operated rats were treated with three transections in the same locations as the ileal interposition group, which were immediately re-joined by anastomosis.

Oral Glucose Tolerance Test (OGTT)

The rats were fasted overnight for a period of 16 hrs, then administered an oral gavage of glucose (20% D-glucose; 1g/kg; Sigma-Aldrich, St. Louis, MO, USA). Before administration of the glucose bolus, baseline blood samples were obtained from the tail vein for measurement of fasting glucose and insulin. Blood glucose was measured with handheld glucometers in duplicate (TheraSense Freestyle Glucometers, Abbott, Chicago, IL, USA) at 15, 30, 45, 60 and 120 minutes from tail blood. Plasma was collected after centrifugation and stored at -80°C until use for measuring insulin level.

Pair Feeding (PF)

Wild type (WT) rats and knock-out (KO) rats were fed ad libitum with rodent chow. The food hoppers in the WT rat cages were weighed (to the nearest tenth of a gram) and were then subtracted from the previous day's hopper weight to determine the amount of food (grams) consumed daily. The daily food intake from WT rats averaged and was used as the amount of

respective diet given to the pair-fed (PF) rats daily. Because the food given to the PF rats was based on that consumed by the WT rats, pair-feeding began one day later for the pair-fed groups. Because PF rats were also *Mc4r* deficient, they quickly consumed all of the allotted food that they were provided. There was no remaining food left in the bedding. Pair feeding was utilized to rule out the influence of body weight differences and to determine whether the improved glucose tolerance was a result of changes in weight. Pair feeding was discontinued at POD 35.

Insulin ELISAs

Insulin concentration were measured with an Ultra-Sensitive Rat Insulin ELISA Kit (Crystal Chem Inc, Downers Grove, IL, USA), and the assay was performed according to the manufacturer's protocol. Briefly, plasma was thawed and divided into aliquots in duplicate for the measurements of plasma insulin. A total of 95 µl of sample diluent per well was dispensed into an antibody-coated microplate, and then 5 µl of the sample per well was added. The microplate was incubated for 2 hours at 4°C. After wells were washed five times with buffer solution, 100 µl of anti-insulin enzyme conjugate per well was added. After 30 minutes of incubation at room temperature, the microplate was washed seven times with wash buffer. A total of 100 µl of enzyme substrate solution per well was dispensed and the microplate was incubated at room temperature while avoiding exposure to light for 40 minutes. Then, 100 µl of enzyme reaction stop solution per well was added to stop the reaction, and measurements were collected at 450 nm and 620 nm using a Multiskan Plus plate reader (Thermo Electron Corporation, Waltham, MA, USA). The result with a correlation coefficient above 95% and a CV below 20% was accepted.

EchoMRI

Fat and lean mass and percentage were determined by nuclear magnetic resonance at both POD 30 and POD 161 (EchoMRI-900 3-in-1, Echo Medical Systems, Houston, TX, USA). Live conscious rats were inserted into an appropriate Plexiglas animal tube and placed into the EchoMRI machine.

Homeostatic Model Assessment For Insulin Resistance

Homeostasis model assessment for insulin resistance (HOMA-IR) was calculated for all rats using the HOMA formula: HOMA-IR = Fasting insulin (mU/L) × plasma glucose (mg/dL) ÷ 405. The HOMA IR result correlated with hyperinsulinemic-euglycemic clamp results (r = 0.88) [20].

Statistics

All statistics were performed in Prism 5 statistical software by GraphPad, and significance was set at * $p < 0.05$, ** $p < 0.01$, and *** $p < 0.001$. Body weight, glucose, insulin and body composition were analyzed by two-way ANOVA with repeated measures. HOMA insulin resistance was analyzed by one-way ANOVA.

RESULTS

Loss of Mc4r function in rats induced obesity

The body weight of KO Sham, KO IT, PF Sham and PF IT was significantly higher than that of WT Sham and WT IT from the 8th week in both male rats (Figure 2A) and from the 6th week in female rats respectively (Figure 2B) (***p<0.001, **p<0.01, and *p<0.05). On POD 30, the body weight of KO Sham and KO IT was significantly higher than that of WT Sham, WT IT, PF Sham and PF IT in both male (Figure 2C) and female rats (Figure 2D) (**p<0.01, and *p<0.05). After the discontinuation of pair feeding (POD 35), the body weight in both the PF Sham and PF IT groups increased gradually to the same weight as that of the KO Sham and KO IT groups in both male (Figure 2A) and female rats (Figure 2B) on POD 161. On POD 161, the body weight of KO Sham, KO IT, PF Sham and PF IT was significantly higher than that of WT Sham and WT IT in both male (Figure 2C) and female rats (Figure 2D) (***p<0.001). The body weight of WT Sham and WT IT, KO Sham and KO IT, PF Sham and PF IT groups in both male (Supplementary figure 1A~1C) and female rats (Supplementary figure 1D~1F) were not significantly different during the experiment period. Body weight was analyzed by two-way

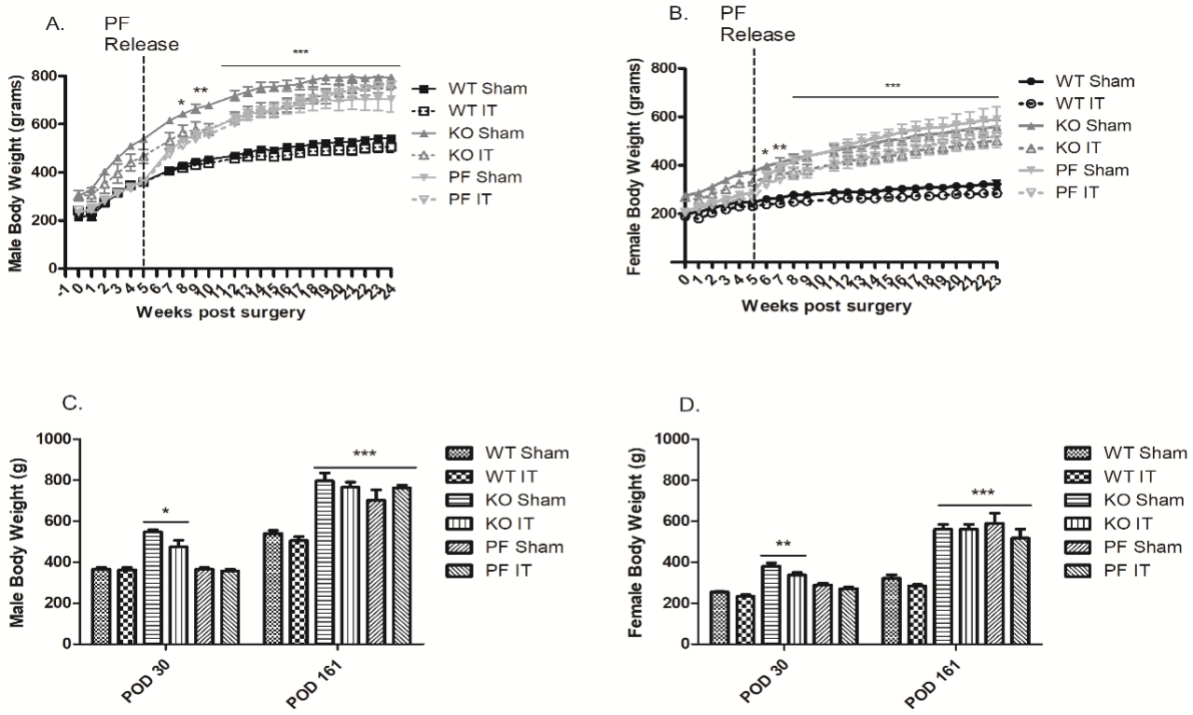

ANOVA with repeated measures.

Figure 2. Loss of *Mc4r* function in the rat induced obesity.

Male KO Sham, not female KO Sham, showed impaired glucose tolerance.

Glucose excursions in response to oral glucose administration were significantly higher in male KO Sham rats at 15, 30, 45, and 60 minutes, as compared with the excursions in the other five male groups (***p<0.001; Figure 3A), while glucose levels in all six female groups were not significantly different during the OGTT (Figure 3B). The secretion of insulin in the KO Sham and PF Sham groups was significantly higher than that in the WT Sham, WT IT, KO IT

and PF IT groups at 0, 45 and 60 minutes in males (**p<0.01, Figure 3C); the secretion of insulin in the KO Sham, KO IT, PF Sham and PF IT groups was significantly higher than that in the WT Sham and WT IT groups at 45 minutes in females (*p<0.05; Figure 3D). Glucose and

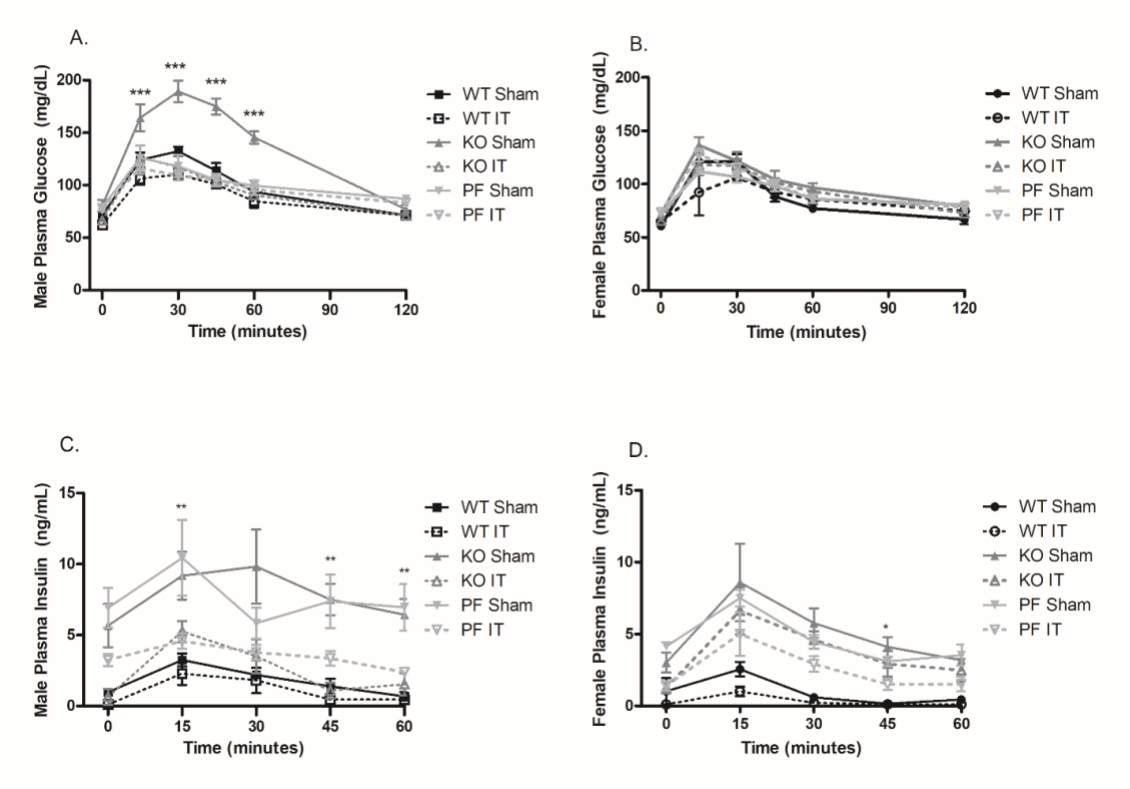

insulin were analyzed by two-way ANOVA with repeated measures.

Figure 3. Male KO Sham, not female KO Sham, showed impaired glucose tolerance.

IT surgery increased insulin sensitivity in both male and female rats independent of genotype

For both male and female rats, the insulin resistance in the KO Sham group was significantly higher than that in the KO IT group; the insulin resistance in the PF Sham group was significantly higher than that in the PF IT group (**p<0.01, *p<0.05; Figure 4A and 4B) on POD 28. The insulin resistance of male KO Sham and PF Sham is higher than that of female KO Sham and PF Sham. HOMA insulin resistance was analyzed by one-way ANOVA.

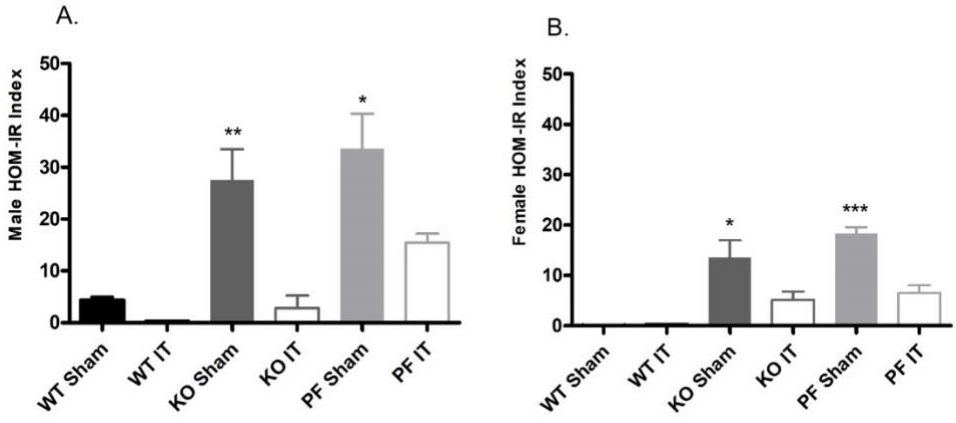

Figure 4. The insulin resistance.

IT surgery decreased both fat percentage and fat mass in female rats but not in male rats on POD 161

For male rats, both fat percentage (Figure 5A) and fat mass (Figure 5B) of KO Sham were significantly higher than those of the other five groups on POD 30 (***p<0.001); on POD 161, both fat percentage (Figure 5A) and fat mass (Figure 5B) of KO Sham, KO IT, PF Sham and PF IT groups were significantly higher than those of WT Sham and WT IT (***p<0.001). No significant difference in either fat percentage or fat mass was found between the WT Sham and WT IT, KO Sham and KO IT, and PF Sham and PF IT groups on POD 161.

For female rats, both fat percentage (Figure 5C) and fat mass (Figure 5D) of KO Sham group were significantly higher than those of the other five groups on POD 30 (*p<0. 05); both fat percentage (Figure 5C) and fat mass (Figure 5D) of KO IT and PF Sham were significantly higher than those of WT Sham, WT IT and PF IT on POD 30 (@p<0.01; Figure 5C). On POD 161, both fat percentage (Figure 5C) and fat mass (Figure 5D) of WT Sham and WT IT groups were significantly lower than those in the KO Sham, KO IT, PF Sham and PF IT groups (***p<0.001); both fat percentage (Figure 5C) and fat mass (Figure 5D) of WT IT, KO IT and PF IT groups were significantly lower than those of WT Sham, KO Sham and PF Sham groups, respectively ($p<0.05). Fat percentage and fat mass were analyzed by two-way ANOVA with repeated measures.

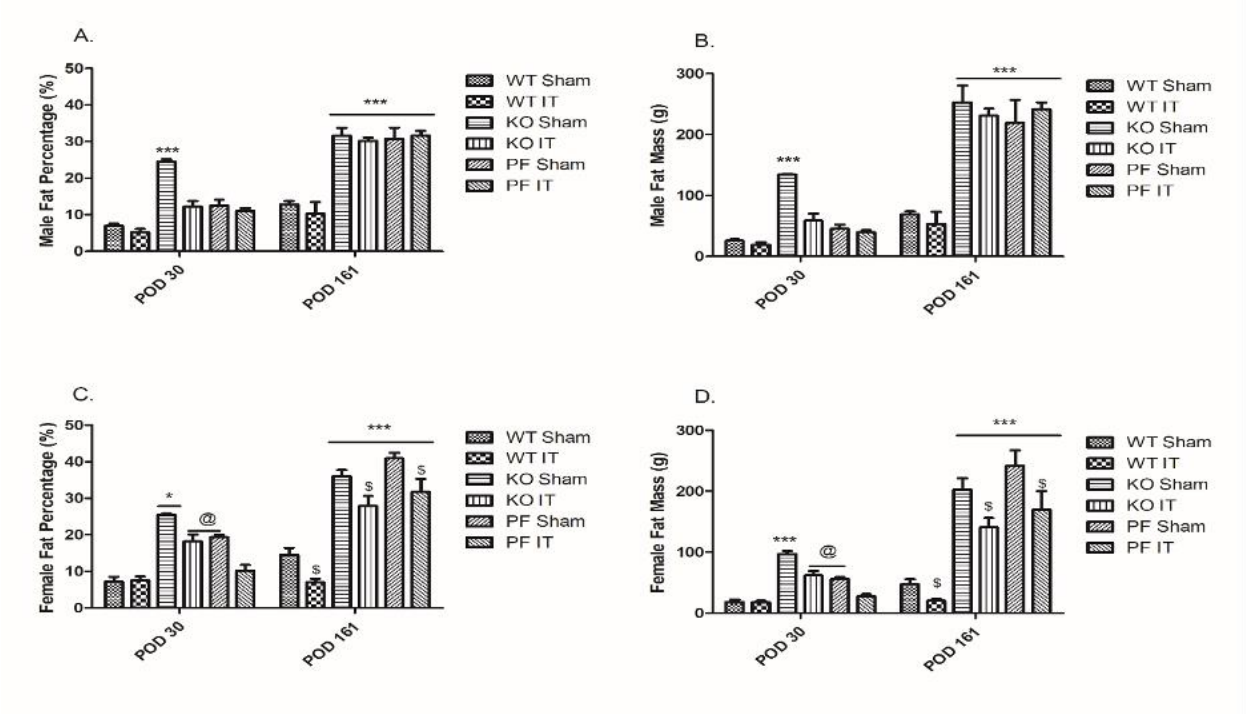

Figure 5. IT surgery decreased both fat percentage and fat mass in female rats, but not in male rats.

IT surgery did not affect lean percentage or lean mass

For male rats on POD 30, the lean percentage (Figure 6A) of WT Sham and WT IT was significantly higher than that in the KO Sham group (***p<0.001); on POD 161, the lean

percentage (Figure 6A) in WT Sham and WT IT was significantly higher than that of KO Sham, KO IT, PF Sham and PF IT groups (*p<0.05). The lean mass (Figure 6B) of KO Sham and KO IT was significantly higher than that of WT Sham, WT IT, PF Sham and PF IT on both POD 30 and POD 161 (***p<0.001, *p<0. 05).

For female rats on POD 30, the lean percentage (Figure 6C) of WT Sham and WT IT was significantly higher than that of KO Sham, KO IT and PF Sham (*p<0. 05); on POD 161, the lean percentage (Figure 6C) of WT Sham and WT IT was significantly higher than that of KO Sham, KO IT, PF Sham and PF IT (***p<0.001, *p<0.05). No significant differences were found in lean mass (Figure 6D) in all six groups on both POD 30 and POD 161. Lean percentage and lean mass were analyzed by two-way ANOVA with repeated measures.

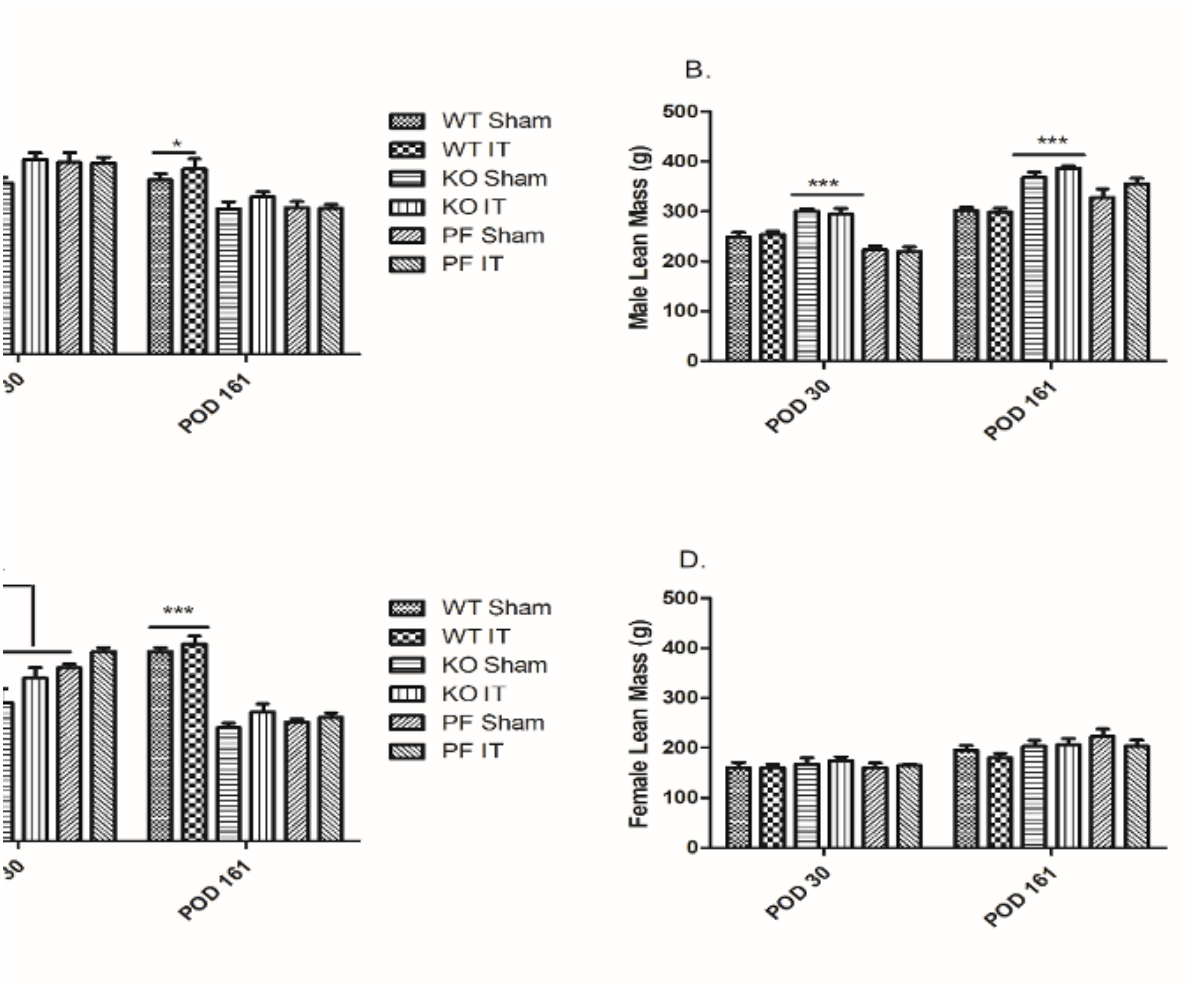

Figure 6. IT surgery did not affect lean percentage or lean mass.

DISCUSSION

Patients with pathogenic MC4R mutation show early-onset obesity and hyperphagia21, 22; We used rats, instead of mice, because the phenotype of Mc4r deficiency in mice, unlike MC4R deficiency in human and Mc4r deficiency in rats, is associated with hyperglycemia and hyperinsulinemia that precede the onset of obesity 4, 23.

Our data indicated that glucose tolerance of male KO rats was improved after IT surgery and IT surgery also increased the insulin sensitivity in both the male and female rats on about 30 days after the surgery, which suggests that Mc4r signaling might not be required for improved glucose tolerance or insulin sensitivity after IT surgery in both male and female KO rats. As we expected, the beneficial effect of glucose metabolism after IT surgery was independent of body weight loss15. Unlike the male KO Sham rats, female KO Sham rats did not show impaired glucose tolerance, which is consistent with the conclusion that males are more insulin resistant than females in both humans 24, 25 and different rodent models 26-29. In both women and female rats, the hormone estradiol (E2) has an anorexigenic function in the central nervous system through direct action in the hypothalamus and prevents the development of obesity and the onset of impaired glucose tolerance 30, 31. We also found that loss of Mc4r signaling led to insulin resistance in both male and female KO rats, which is also consistent with findings from previous studies 32, 33. Similar outcomes between PF and ad lib groups (Fig 4) suggested that IT surgery, but not the intermittent fasting (or meal feeding), may correct MC4R deficiency-induced insulin resistance.

We further expanded our study by adding both male and female PF groups to examine whether body weight is a factor affecting insulin resistance and whether IT surgery might increase insulin sensitivity in PF groups. We found that Mc4r mutation caused increased insulin resistance in both male and female PF rats on postoperative day 28 when the body weight and glucose of PF groups were almost the same as those of WT rats, which indicates that Mc4r might control the insulin resistance independent of body weight and glucose level. Additionally, IT surgery decreased insulin resistance significantly in both male and female PF rats. It might be due to the increased level of glucagon-like peptide 1 (GLP-1), fibroblast growth factor (FGF) 15/19 and FGF 21 after the IT surgery34, 35, 15, 36, 37.

Our results are consistent with previous studies that Mc4r mutation increased fat mass and/or percentage in male rats 13, 38; the mutation caused the same effect in female rats. IT surgery maintained the decreased fat mass and percentage in female rats, not male rats, on postoperative day (POD) 161; POD 161 in rats is equivalent to 18 years post surgery in humans 39. Therefore, the surgery has a lasting effect in female rats, not in male rats. This effect might be due to sexual dimorphism in fat accumulation; both human and rat females have a higher percentage of fat than age-matched males, but females accumulate more subcutaneous fat, whereas males accumulate more visceral fat 29. The mechanism by which IT surgery decreases the fat mass and percentage in only female rats needs further study.

In conclusion, our data suggest that Mc4r signaling is not necessary for the effect of ileal interposition on glucose homeostasis and insulin resistance; female rats, not male rats, maintained decreased fat mass and percentage for the duration of the study after IT surgery.

ACKNOWLEDGMENTS

The present study was supported by funds to Dr. Strader from NIDDK – Challenge grant 1RC1DK086999 and is in memory of her. Grant (No. 42903) for Ping Zhao from University of North Alabama College of Arts & Sciences also contributes to the project. Thanks for the suggestions and help from Kai Xue in Ruijin Hospital Affiliated to Shanghai Jiao Tong University School of Medicine, Shanghai, China.

REFERENCES

1. Cone RD. The central melanocortin system and energy homeostasis. Trends in Endocrinology & Metabolism. 1999;10(6):211-16.
2. Tao Y-X. The melanocortin-4 receptor: physiology, pharmacology, and pathophysiology. Endocrine reviews. 2010;31(4):506-43.
3. Berglund ED, Liu T, Kong X, Sohn J-W, Vong L, Deng Z, et al. Melanocortin 4 receptors in autonomic neurons regulate thermogenesis and glycemia. Nature Neuroscience. 2014 2014/07/01;17(7):911-13.
4. Huszar D, Lynch CA, Fairchild-Huntress V, Dunmore JH, Fang Q, Berkemeier LR, et al. Targeted disruption of the melanocortin-4 receptor results in obesity in mice. Cell. 1997;88(1):131-41.
5. Farooqi IS, O'Rahilly S. Genetics of obesity in humans. Endocrine reviews. 2006;27(7):710-18.
6. Loos RJ. The genetic epidemiology of< i> melanocortin 4 receptor</i> variants. European journal of pharmacology. 2011;660(1):156-64.
7. Collet T-H, Dubern B, Mokrosinski J, Connors H, Keogh JM, de Oliveira EM, et al. Evaluation of a melanocortin-4 receptor (MC4R) agonist (Setmelanotide) in MC4R deficiency. Molecular metabolism. 2017;6(10):1321-29.
8. Buchwald H, Avidor Y, Braunwald E, Jensen MD, Pories W, Fahrbach K, et al. Bariatric surgery: a systematic review and meta-analysis. Jama. 2004;292(14):1724-37.
9. Pories WJ, Swanson MS, MacDonald KG, Long SB, Morris PG, Brown BM, et al. Who would have thought it? An operation proves to be the most effective therapy for adult-onset diabetes mellitus. Ann Surg. 1995 Sep;222(3):339-50; discussion 50-2.
10. Aslan I, Ranadive SA, Ersoy BA, Rogers SJ, Lustig RH, Vaisse C. Bariatric surgery outcome in a patient with complete MC4R deficiency. International journal of obesity (2005). 2011;35(3):457.
11. Censani M, Conroy R, Deng L, Oberfield SE, McMahon DJ, Zitsman JL, et al. Weight loss after bariatric surgery in morbidly obese adolescents with MC4R mutations. Obesity. 2014;22(1):225-31.
12. Zechner JF, Mirshahi UL, Satapati S, Berglund ED, Rossi J, Scott MM, et al. Weight-independent effects of roux-en-Y gastric bypass on glucose homeostasis via melanocortin-4 receptors in mice and humans. Gastroenterology. 2013;144(3):580-90. e7.
13. Mul JD, Begg DP, Alsters SI, van Haaften G, Duran KJ, D'Alessio DA, et al. Effect of vertical sleeve gastrectomy in melanocortin receptor 4-deficient rats. American Journal of Physiology-Endocrinology And Metabolism. 2012;303(1):E103-E10.

14. Zhao P, Wendt D, Goodin SZ, Ravichandran S, Chouinard TE, Strader AD. Adaptation of Intestinal and Bile Acid Physiology Accompany the Metabolic Benefits Following Ileal Interposition in the Rat. Obesity Surgery.1-10.
15. Strader AD, Clausen TR, Goodin SZ, Wendt D. Ileal interposition improves glucose tolerance in low dose streptozotocin-treated diabetic and euglycemic rats. Obesity surgery. 2009;19(1):96-104.
16. Strader AD. Ileal transposition provides insight into the effectiveness of gastric bypass surgery. Physiology & behavior. 2006;88(3):277-82.
17. Buchwald H, Estok R, Fahrbach K, Banel D, Sledge I. Trends in mortality in bariatric surgery: a systematic review and meta-analysis. Surgery. 2007;142(4):621-35.
18. van Boxtel R, Vroling B, Toonen P, Nijman IJ, van Roekel H, Verheul M, et al. Systematic generation of in vivo G protein-coupled receptor mutants in the rat. The pharmacogenomics journal. 2011;11(5):326-36.
19. Obici S, Magrisso IJ, Ghazarian AS, Shirazian A, Miller JR, Loyd CM, et al. Moderate voluntary exercise attenuates the metabolic syndrome in melanocortin-4 receptor-deficient rats showing central dopaminergic dysregulation. Molecular metabolism. 2015;4(10):692-705.
20. Matthews D, Hosker J, Rudenski A, Naylor B, Treacher D, Turner R. Homeostasis model assessment: insulin resistance and β-cell function from fasting plasma glucose and insulin concentrations in man. Diabetologia. 1985;28(7):412-19.
21. Lubrano-Berthelier C, Dubern B, Lacorte J-M, Picard F, Shapiro A, Zhang S, et al. Melanocortin 4 receptor mutations in a large cohort of severely obese adults: prevalence, functional classification, genotype-phenotype relationship, and lack of association with binge eating. The Journal of Clinical Endocrinology & Metabolism. 2006;91(5):1811-18.
22. Calton MA, Ersoy BA, Zhang S, Kane JP, Malloy MJ, Pullinger CR, et al. Association of functionally significant Melanocortin-4 but not Melanocortin-3 receptor mutations with severe adult obesity in a large North American case–control study. Human molecular genetics. 2009;18(6):1140-47.
23. Marie LS, Miura GI, Marsh DJ, Yagaloff K, Palmiter RD. A metabolic defect promotes obesity in mice lacking melanocortin-4 receptors. Proceedings of the National Academy of Sciences. 2000;97(22):12339-44.
24. Nuutila P, Knuuti MJ, Mäki M, Laine H, Ruotsalainen U, Teräs M, et al. Gender and insulin sensitivity in the heart and in skeletal muscles: studies using positron emission tomography. Diabetes. 1995;44(1):31-36.
25. Mittendorfer B. Insulin resistance: sex matters. Current Opinion in Clinical Nutrition & Metabolic Care. 2005;8(4):367-72.
26. Clark JB, Palmer CJ, Shaw WN. The diabetic Zucker fatty rat. Proceedings of the Society for Experimental Biology and Medicine. 1983;173(1):68-75.
27. Zierath JR, Houseknecht KL, Gnudi L, Kahn BB. High-fat feeding impairs insulin-stimulated GLUT4 recruitment via an early insulin-signaling defect. Diabetes. 1997;46(2):215-23.
28. Li AC, Brown KK, Silvestre MJ, Willson TM, Palinski W, Glass CK. Peroxisome proliferator–activated receptor γ ligands inhibit development of atherosclerosis in LDL receptor–deficient mice. Journal of Clinical Investigation. 2000;106(4):523.
29. Macotela Y, Boucher J, Tran TT, Kahn CR. Sex and depot differences in adipocyte insulin sensitivity and glucose metabolism. Diabetes. 2009;58(4):803-12.

30. Clegg DJ, Brown LM, Woods SC, Benoit SC. Gonadal hormones determine sensitivity to central leptin and insulin. Diabetes. 2006;55(4):978-87.
31. Roepke TA. Oestrogen modulates hypothalamic control of energy homeostasis through multiple mechanisms. Journal of neuroendocrinology. 2009;21(2):141-50.
32. Fan W, Dinulescu DM, Butler AA, Zhou J, Marks DL, Cone RD. The central melanocortin system can directly regulate serum insulin levels. Endocrinology. 2000;141(9):3072-79.
33. Obici S, Feng Z, Tan J, Liu L, Karkanias G, Rossetti L. Central melanocortin receptors regulate insulin action. Journal of Clinical Investigation. 2001;108(7):1079-85.
34. Drucker DJ, Nauck MA. The incretin system: glucagon-like peptide-1 receptor agonists and dipeptidyl peptidase-4 inhibitors in type 2 diabetes. Lancet. 2006 Nov 11;368(9548):1696-705.
35. Patti ME, Houten SM, Bianco AC, Bernier R, Larsen PR, Holst JJ, et al. Serum bile acids are higher in humans with prior gastric bypass: potential contribution to improved glucose and lipid metabolism. Obesity. 2009;17(9):1671-77.
36. Mencarelli A, Renga B, D'Amore C, Santorelli C, Graziosi L, Bruno A, et al. Dissociation of intestinal and hepatic activities of FXR and LXRα supports metabolic effects of terminal ileum interposition in rodents. Diabetes. 2013;62(10):3384-93.
37. Yan K, Chen W, Zhu H, Lin G, Pan H, Li N, et al. Ileal transposition surgery decreases fat mass and improves glucose metabolism in diabetic GK rats: possible involvement of FGF21. Frontiers in physiology. 2018;9:191.
38. Mul JD, Boxtel R, Bergen DJ, Brans MA, Brakkee JH, Toonen PW, et al. Melanocortin receptor 4 deficiency affects body weight regulation, grooming behavior, and substrate preference in the rat. Obesity. 2012;20(3):612-21.
39. Andreollo NA, Santos EFd, Araújo MR, Lopes LR. Rat's age versus human's age: what is the relationship? ABCD Arquivos Brasileiros de Cirurgia Digestiva (São Paulo). 2012;25(1):49-51.

Journal of Alabama Academy of Science, Vol. 92, No. 2, November 2021

AN EXAMINATION OF THE SUNSPOT AREAL DATASET, 1875–2017: PAPER II, HEMISPHERIC DIFFERENCES

Robert M. Wilson
NASA Marshall Space Flight Center, NSSTC, Huntsville, Alabama

robert.m.wilson@nasa.gov

ABSTRACT

This is the second paper in an anticipated three-part study of the sunspot areal dataset. Examined are the annual variations of the northern (N) and southern (S) hemispheric sunspot area (SSA), number of active region entries (NARE), and the mean area per entry (MAE) for the interval 1875–2017, spanning solar cycles (SCs) SC12–SC24. For the overall interval of 1875–2019, SSA(N) has been larger than SSA(S) for 77 of the 145 years. Likewise, for SC12–SC24, SSA(N) has been greater than SSA(S) during the ascending phase of the solar cycle (i.e., 35 of 52 years), whether the SC is an even- or odd-numbered SC, while SSA(S) has been greater than SSA(N) during the descending phase of the solar cycle (51 of 93 years). Minimum SSA(N) and SSA(S) have occurred in the same year in only 7 of 13 SCs, including SC14, SC16 and SC19–SC23. Maximum SSA(N) and SSA(S) have occurred in the same year only once (in SC15). Maximum SSA(S) usually occurs after maximum SSA(N), true for 9 of 13 SCs. Maximum SSA(S) preceded maximum SSA(N) in SC16, SC18, and SC19. Multiple peaks in SSA(N) or SSA(S), typically 2–3 years apart, have often been seen (e.g., SC12–SC16 and SC18–SC22). SC12 had the smallest maximum SSA(N) (452.0 millionths of a solar hemisphere), while SC19 had the largest maximum SSA(N) (2,277.2 millionths of a solar hemisphere). SC14 had the smallest SSA(S) (600.3 millionths of a solar hemisphere), while SC18 had the largest SSA(S) (1,642.9 millionths of a solar hemisphere). The average time from minimum to maximum SSA(N) is 3.8 years (range 2–5 years), while it is 4.8 years for SSA(S) (range 3–6 years). The average time from maximum SSA(N) to the following minimum SSA(N) is 6.9 years (range 5–9 years), while it is 6.2 years for SSA(S) (range 5–8 years). The largest N-S asymmetry coefficients for SSA occurs between –3 and +1 years about sunspot minimum. The largest N-S asymmetry coefficient in SSA occurred in 2019 (SC24). The largest area sunspot occurred in 1947 (SC18) in the southern hemisphere and measured 6,132 millionths of a solar hemisphere, nearly twice the size of the average maxima of the largest area spots in the other 12 SCs. SSA and NARE are highly correlated with each other and with SSN. Minimum MAE(N) and MAE(S) may have occurred, respectively, in 2018 and 2019, highly suggestive that SSN(m) for SC25 either occurred in 2019 or will occur in 2020.

INTRODUCTION

This is the second paper in an anticipated three-part study of the sunspot areal dataset, 1875–2017. Paper I (Wilson 2020) provided a general overview of the sunspot areal dataset, examining—in particular—the annual variations of selected parameters and inferred correlations that are apparent in the sunspot areal dataset. This paper (Paper II) examines the hemispheric

differences of selected parameters using the sunspot areal database. Paper III will examine annual variations of the magnetic complexity of sunspots.

North-South (N-S) asymmetry has long-been recognized by solar observers as related to the distributions of major flare events, sunspot magnetic classes and sunspot areas. For example, Newton and Milson (1955) studied the N-S asymmetry of sunspot areas during the interval 1874–1954 and concluded that the fluctuations are real, their work following previous work reported by Newcomb (1901), Maunder (1922) and Kiepenheuer (1953). Later, Waldmeier (1971) investigated the N-S asymmetry of sunspots during the interval 1874–1969, arguing that the real asymmetry was strengthened by a phase difference of the two hemispheres, where the phase shift is subject to a long period that contains eight 11-year SCs. Roy (1977) noted that magnetically complex sunspot groups displayed a more pronounced asymmetry during the interval 1962–1970 than noncomplex groups. Antalová and Gnevyshev (1983) found that an N-S sunspot area asymmetry was a persistent feature, especially for SC14–SC20. Swinson et al. (1986) noted that, in general, northern hemispheric activity peaked about 2 years after sunspot minimum, with even-numbered cycles having a greater peak in northern hemispheric activity. Vizoso and Ballester (1987) examined the N-S asymmetry in sudden disappearances of solar prominences, noting that it does not appear to be in phase with the solar cycle, instead peaking about the time of solar minimum and reversing in sign during solar maximum. Garcia (1990) noted that the N-S distribution of large flares appears periodic and approximately in phase with the solar cycle, with the most intense large flares showing the largest N-S asymmetry. Vizoso and Ballester (1990) performed an exhaustive study of the N-S asymmetry of sunspots during the interval 1874–1976 and found: (1) that the N-S asymmetry is statistically significant, (2) the highest values of the N-S asymmetry coefficient for sunspots are obtained around sunspot minimum, and (3) there is a long-term periodic behavior of about eight cycles in which the activity in one hemisphere is more important during the ascending branch while during the descending branch the activity becomes more important in the opposite hemisphere. Through the years, many other studies have followed, investigating the N-S asymmetry of sunspots/solar flares including, in part: Schlamminger (1991); Yi (1992); Carbonell et al. (1993); Oliver and Ballester (1994); Duchlev and Dermendjiev (1996); Watari (1996); Ataç and Özgüç (1996); Vernova et al. (2002); Temmer et al. (2002, 2006); Li, Wang, Xiong, et al., (2002); Li, Chen, Zhan, Shi et al. (2009); Li, Gao, Zhan (2008); Li, Gao, Zhan et al. (2009); Knaack et al. (2004); Joshi and Joshi (2004); Vernova et al. (2004); Ballester et al. (2005); Zharkov et al. (2005); Zolotova and Ponyavin (2006); Zolotova and Ponyavin (2007); Chang (2007, 2008); Li (2009); Donner and Thiel (2007); Zolotova et al. (2009); Badalyan and Obridko (2011); and Chowdhury et al. (2013).

In this Paper (II), several issues regarding the asymmetry of sunspots are examined, including: (1) the variation of the N and S hemispheric annual SSAs for the interval 1875–2017 in relation to SSN minimum (m) and maximum (M) occurrences, (2) the variation of the N- and S-hemispheric annual NARE, (3) the variation of N- and S-hemispheric annual MAE, (4) the annual asymmetry coefficients for SSA and NARE, and (5) the results of epoch analyses for these parameters based on SSN(m) occurrence.

METHODS AND MATERIALS

Two primary data sources are used in this study: (1) annual values of SSN, available online at http://sidc.oma.be/silo/datafiles and (2) annual values of SSA, available online at http://solarcyclescience.com/activeregions.html. Other parameters taken from the SSA dataset

(Greenwich Observatory (RGO) interval 1875–1976) and the United States Air Force/National Oceanic and Atmospheric Administration (USAF/NOAA) interval 1977–2019) include (1) NARE and (2) MAE, where MAE is computed as SSA divided by NARE times the number of days in the year.

RESULTS AND DISCUSSION

Table 1 provides the basic data used in this investigation, spanning the interval 1875–2017. The yearly 2018 and 2019 values are also shown but have not been included in the parametric means, which are given at the bottom of the table, both in terms of overall means (and standard deviations, *sd*) and even- and odd-numbered sunspot cycle means (and *sd*). Given in table 1 are the (1) NARE, (2) SSA, (3) MAE, and (4) asymmetry for NARE and SSA. For NARE, SSA, and MAE, the yearly N hemispheric, S hemispheric, and combined (C) hemispheric parametric values are given. Also given is each cycle's largest observed area (active region), denoted LAAR, and the hemisphere (H) in which it occurred. Also identified are the m and M parametric values for each SC, SC12–SC24.

Table 1. N-S hemispheric values of NARE, SSA and MAE, along with SSN, LAAR/H and asymmetry of NARE and SSA, 1875–2017.

		NARE			SSA			MAE				Asymmetry	
Year	SSN	C	N	S	C	N	S	C	N	S	LAAR/H	NARE	SSA
1875	28.3	394	222	172	213.1	123.0	90.2	197	202	191	981/N	0.127	0.154
1876	18.9	265	83	182	109.3	34.6	74.7	151	153	150	711/S	–0.374	–0.367
1877	20.7	229	106	123	92.9	35.4	57.4	148	122	170	778/S	–0.074	–0.237
SC12													
1878	5.7m	81m	66	15m	22.2m	20.5	1.7m	100m	113	41m	402/N,m	0.630M	0.847M
1879	10.0	117	53m	64	36.3	11.9m	24.4	113	82m	139	464/S	–0.094M	–0.344
1880	53.7	775	467	308	446.8	271.4	175.3	211	213M	208	1,449/N	0.205	0.215
1881	90.5	1,423	894	529	679.5	452.0M	227.5	174	185	157	1,227/N	0.257	0.330
1882	99.0	1,622	895M	727	968.0	441.9	526.1	218	180	264	2,425/N,M	0.104	–0.087m
1883	106.1M	1,792	661	1,131	1,148.9M	328.0	820.9M	234M	181	265M	1,876/N	–0.262	–0.429
1884	105.8	2,039M	833	1,206M	1,034.1	451.3	582.8	186	198	177	2,246/S	0.183	–0.127
1885	86.3	1,522	505	1017	810.2	282.9	527.3	194	204	189	1,917/M	–0.336	–0.302
1886	42.4	750	239	511	379.4	97.4	282.0	185	149	201	1,125/M	–0.363	–0.487
1887	21.8	452	145	307	177.3	43.4	133.9	143	109	159	1,030/S	–0.358	–0.510
1888	11.2	265	50	215	87.9	19.5	68.5	121m	143	116m	786/S	–0.623	–0.557
SC13													
1889	10.4m	191m	29m	162	76.7m	4.7m	72.0	147	59m	162	639/S,m	–0.696M	–0.877M
1890	11.8	258	116	142m	98.9	53.4	45.4m	140	168	117	1,135/S	–0.101	0.081
1891	59.5	1,252	881	371	566.4	399.1	167.4	165	165	165	1,798/N	0.407	0.409
1892	121.7	2,321	1,193	1,128	1,211.3	602.0M	609.2	191	185	198	3,038/S,M	0.028	–0.006m
1893	142.0M	3,072M	1,264M	1,808M	1,460.6M	516.6	944.0M	174	149	191	2,621/S	–0.177	–0.293
1894	130.0	2,740	1,258	1,482	1,281.5	544.6	736.9	171	158	181	2,511/S	–0.082	–0.150
1895	106.6	2,134	1,076	1,058	973.4	567.5	406.0	166	193	140	1,722/S	0.008m	0.285
1896	69.4	1,182	379	803	547.4	206.0	341.5	169	199M	157	2,458/N	–0.359	–0.248
1897	43.8	903	393	510	511.7	182.8	328.9	207M	170	235M	2,743/S	–0.130	–0.286
1898	44.4	777	271	506	374.7	108.5	266.2	176	146	192	2,235/S	–0.302	–0.421
1899	20.2	385	86	299	110.0	23.4	86.6	104	99	106	638/S,m	–0.553M	–0.575M
1900	15.7	273	120	153	74.3	26.8	47.5	100m	82m	114	750/S	–0.121	–0.279
SC14													
1901	4.6m	78m	36m	42m	27.9m	21.2m	6.6m	131	215	57m	699/N	–0.077m	0.523
1902	8.5	134	87	47	59.5	39.9	19.6	162	167	152	1,113/N	0.299	0.341
1903	40.8	760	330	430	338.6	131.5	207.1	163	145	176	2,129/S	–0.132	–0.223
1904	70.1	1,374	825	549	488.2	268.5	219.7	130	119	146	1,532/N	0.201	0.100
1905	105.5M	1,937	1,145	792	1,195.9M	749.3M	446.6	225M	239M	206	3,339/S,M	0.182	0.253
1906	90.1	1,859	1,235M	624	775.0	535.5	239.5	152	158	140	1,470/S	0.329	0.382
1907	102.8	1,951M	898	1,053M	1,092.1	491.8	600.3M	204	200	208M	2,555/S	–0.079	–0.099
1908	80.9	1,687	698	989	697.5	316.5	381.0	151	166	141	1,919/N	–0.172	–0.092m
1909	73.2	1,442	577	865	691.5	297.0	394.5	175	188	166	1,959/S	–0.200	–0.141

		NARE			SSA			MAE				Asymmetry	
Year	SSN	C	N	S	C	N	S	C	N	S	LAAR/H	NARE	SSA
1910	30.9	766	207	559	266.0	64.8	201.3	127	114	131	1,139/S	–0.460	–0.513
1911	9.5	279	78	201	64.4	21.6	42.8	84	101	78	332/N	–0.441	–0.329
1912	6.0	154	11m	143	37.3	0.8m	36.6	89	127m	94	685/S	–0.857M	–0.960M
SC15													
1913	2.4m	60m	39	21m	7.5m	5.1	2.5m	46m	48	43m	138/N,m	0.300	0.347
1914	16.1	436	225	211	152.4	99.1	53.3	128	161	92	817/N	0.032	0.301
1915	79.0	1,864	1,012	852	697.8	380.2	317.6	137	137	136	1,901/S	0.086	0.090m
1916	95.0	2,290	1,414	876	725.5	470.0	255.4	116	122	107	1,775/N	0.235	0.296
1917	173.6M	3,510M	1,938M	1,572M	1,533.9M	853.6M	680.4M	160	161	158	3,590/S,M	0.104	0.113
1918	134.6	2,904	1,500	1404	1,112.6	608.3	504.3	140	148	131	1,749/S	0.033	0.093
1919	105.7	2,249	991	1258	1,054.7	565.4	489.3	171M	208M	142	1,776N	–0.119	0.072
1920	62.7	1,396	678	718	617.3	207.8	409.5	162	112	209M	2,690/S	–0.029m	–0.327
1921	43.5	943	516	427	419.6	250.2	169.4	162	177	145	1,709/S	0.094	0.193
1922	23.7	543	314	229	252.0	160.0	92.0	169	186	147	1,478/N	0.157	0.270
SC16													
1923	9.7m	244m	138m	106m	54.7m	32.6m	22.0m	82m	86m	76m	831/N,m	0.131	0.194
1924	27.9	589	452	137	278.0	233.7	44.4	173	189	119	1,387/N	0.535M	0.681M
1925	74.0	1,718	1,072	646	825.1	513.7	311.3	175	175	176	2,934/N	0.248	0.245
1926	106.5	2,210	1,107	1,103	1,263.2	661.3	601.8	209M	218M	199M	3,716/N,M	0.002m	0.047m
1927	114.7	2,369	941	1,428M	1,060.8	379.0	681.9M	163	147	174	1,562/N	–0.206	–0.286
1928	129.7M	2,613M	1,301M	1,312	1,388.9M	725.9M	663.0	195	204	185	2,587/S	–0.004	0.045
1929	108.2	2,413	1,256	1,157	1,238.9	650.6	588.3	187	189	186	2,003/N	0.041	0.050
1930	59.4	1,394	798	596	516.6	286.1	230.6	135	131	141	1,506/N	0.145	0.107
1931	35.1	781	514	267	279.1	204.2	74.9	130	145	102	1,882/N	0.316	0.633
1932	18.6	471	283	188	163.2	122.7	40.5	127m	159	79	1,155/N,m	0.202	0.504
SC17													
1933	9.2m	225m	200	25m	91.3	89.5	1.8m	148	163	26m	1,594/N	0.778M	0.961M
1934	14.6	337	156m	181	118.2	44.3m	73.9	128	104m	149	1,169/S	–0.074	–0.250
1935	60.2	1,290	558	732	622.1	203.3	418.8	176	133	209	2,435/S	–0.135	–0.346
1936	132.8	2,706	1,214	1,492	1,140.8	462.6	678.2	154	139	166	1,641/S	–0.103	–0.189
1937	190.6M	3,705M	2,114M	1,591	2,072.8M	1,316.1M	756.7	204	227	174	3,340/N	0.141	0.270
1938	182.6	3,401	1,690	1,711M	2,015.2	886.0	1,129.2M	216	191	241M	3,627/N,M	–0.006m	–0.121
1939	148.0	2,892	1,330	1,562	1,576.8	645.1	931.7	199	177	218	3,054/S	–0.080	–0.182
1940	113.0	2,118	938	1,180	1,037.2	497.0	540.1	179	194	168	2,860/N	–0.114	–0.042m
1941	79.2	1,473	848	625	658.1	434.4	223.7	163	187	131	3,088/N	0.151	0.320
1942	50.8	1,014	527	487	427.3	256.2	171.2	154	177	128	2,048/N	0.039	0.199
1943	27.1	495	343	152M	296.8	250.9	45.9m	219M	267M	110m	1,892/N	0.386M	0.691M
SC18													
1944	16.1m	370m	135m	235	124.7m	42.2m	82.5	123m	114m	128	1,010/S,m	–0.270	–0.323
1945	55.3	1,103	369	734	426.5	119.4	307.2	141	118	153	1,142/S	–0.331	–0.440
1946	154.3	2,838	1,389	1,449	1,823.9	1,116.2	707.7	235M	293M	178	5,202/N	–0.021m	0.224
1947	214.7M	4,298M	1,930	2,368M	2,634.1M	991.1	1,642.9M	224	187	253M	6,132/S,M	–0.102	–0.247
1948	193.0	3,892	1,809	2,083	1,974.6	934.1	1,040.5	186	189	183	2,434/S	–0.070	–0.054m
1949	190.7	3,903	2,177M	1,726	2,140.0	1,180.2M	959.8	200	198	203	2,471/N	0.116	0.103
1950	118.9	2,333	1,396	937	1,227.3	776.2	451.2	192	203	176	2,856/N	0.197	0.265
1951	98.3	1,861	1,044	817	1,135.3	729.9	405.4	223	255	181	4,865/N	0.122	0.286
1952	45.0	963	457	506	402.9	194.7	208.2	153	156	151	1,212/S	–0.051	–0.034
1953	20.1	431	265	166	145.1	105.9	39.2	123	146	86m	1,062/N	0.230	0.460M
SC19													
1954	6.6m	166m	93m	73m	34.6m	11.7m	22.9m	76m	46m	115	712/S,m	0.120	–0.324
1955	54.2	1,183	746	437	552.4	328.5	223.9	170	161	187	1,449/N	0.261M	0.189
1956	200.7	3,820	1,911	1,909	2,394.7	1,242.8	1,151.9	229	238	221	2,306/S	0.001m	0.038m
1957	269.3M	4,855	2,295	2,560M	3,048.5M	1,446.6	1,601.9	229	230	228	2,480/S	–0.055	–0.051
1958	261.7	5,016M	2,630	2,386	3,011.3	1,402.5	1,608.8M	219	195	246M	2,256/N	0.049	–0.069
1959	225.1	4,514	3,173M	1,341	2,872.9	2,277.2M	595.8	232M	262M	162	2,805/N,M	0.406	0.585
1960	159.0	3,259	2,001	1,258	1,641.2	1,051.7	589.5	184	192	172	2,301/N	0.228	0.282
1961	76.4	1,586	1,008	578	613.5	444.5	169.0	141	161	107	1,445/N	0.271	0.449
1962	53.4	1,027	709	318	463.5	324.3	139.2	165	167	160	1,841/N	0.381	0.399
1963	39.9	819	630	189	287.8	228.1	59.7	128	132	115	1,311/N	0.538	0.585
SC20													
1964	15.0m	390m	284m	106	53.9m	44.1m	9.8m	51m	57m	34m	545/S,m	0.456	0.636
1965	22.0	506	429	77m	113.3	97.2	16.1	82	83	76	736/N	0.696M	0.716
1966	66.8	1,498	1,266	232	592.6	535.4	57.2	144	154	90	1,600/N	0.690	0.807M
1967	132.9	3,390M	2,159M	1,231	1,519.1	1,033.6M	485.6	164	175	144	2,235/N	0.274	0.361
1968	150.0M	2,963	1,588	1,375	1,569.8	961.2	608.6	194M	222M	162	3,202/N,M	0.072	0.225
1969	149.4	2,932	1,678	1,254	1,450.1	922.5	527.6	181	201	154	2,274/N	0.145	0.272
1970	148.0	3,379	1,757	1,622M	1,601.3M	918.0	683.3M	173	191	154	2,511/N	0.040	0.147
1971	94.4	2,229	1,121	1,108	990.2	455.0	534.8	162	148	176M	2,330/S	0.006	–0.080

		NARE			SSA			MAE				Asymmetry	
Year	**SSN**	**C**	**N**	**S**	**C**	**N**	**S**	**C**	**N**	**S**	**LAAR/H**	**NARE**	**SSA**
1972	97.6	2,263	877	1,386	916.7	328.4	588.3	148	137	155	2,250/S	–0.225	–0.284
1973	54.1	1,203	596	607	457.6	227.4	230.2	139	139	138	919/N	–0.009m	–0.006m
1974	49.2	1,096	384	712	398.9	138.2	260.6	133	131m	134	2,706/S	–0.299M	–0.307
1975	22.5	473	290	183m	166.4m	122.0	44.5m	128m	154	89m	1,295/N	0.226	–0.466M
SC21													
1976@	18.4m	426m	198m	228	169.8	95.0m	74.8	146	176	120	937/S	–0.070	0.119
1977	39.3	926	580	346	347.0	211.3	135.7	137	133	143	1,170/N	0.253	0.218
1978	131.0	4,035	2,247	1,788	1,368.5	854.5	514.1	124	139	105	1,920/N	0.114	0.249
1979	220.1M	5,438M	2,904M	2,534M	2,194.5	1,289.9M	904.6	147	162	130	1,720/S	0.068	0.176
1980	218.9	3,965	1,936	2,029	2,160.7	933.6	1,227.1M	199	176	221	2,300/S	–0.023m	–0.136
1981	198.9	3,920	2,038	1,882	2,270.2M	1,078.3	1,192.0	211	193	231M	2,301/S	0.040	–0.050
1982	162.4	3,686	1,759	1,927	2,220.1	1,088.9	1,131.3	220M	226	214	3,100/N,M	–0.046	–0.019m
1983	91.0	2,371	699	1,672	919.5	224.8	694.7	142	117	152	2,110/S	–0.410M	–0.511M
1984	60.5	1,474	524	950	811.7	355.8	456.0	202	249M	176	2,590/S	–0.289	–0.123
1985	20.6	604	280	324	179.0	81.2	97.7	108m	106	110	840/N	–0.073	–0.092
SC22													
1986	14.8m	394m	242m	152m	123.2m	80.4m	42.8m	114	121	103m	700/S,m	0.228	0.305
1987	33.9	938	340	598	293.8	97.0	196.8	114	104m	120	800/N	–0.275	–0.340
1988	123.0	2,900	1,591	1,309	1,343.4	674.2	669.1	170	155	187	2,900/S	0.097	0.004
1989	211.1M	4,734	2,532M	2,202	2,572.0M	1,363.8M	1,208.3	198M	197m	200M	3,600/N,M	0.070	0.060
1990	191.8	4,751M	2,202	2,549	2,053.2	1,039.0	1,014.2	158	172	145	3,080/N	–0.073	0.012
1991	203.3	4,715	1,798	2,917M	2,499.2	943.0	1,555.8M	193	192	195	2,530/S	–0.237	–0.245
1992	133.0	3,314	1,287	2,027	1,380.8	553.0	827.9	152	157	149	1,650/S	–0.223	–0.199
1993	76.1	1,886	941	945	717.2	358.7	358.5	138	139	138	1,230/S	–0.002m	0.000m
1994	44.9	1,205	566	639	361.4	215.1	146.3	109	139	84m	940/N	–0.061	0.190
1995	25.1	707	293	414	169.0	61.3	107.7	87m	76	95	1,800/S	–0.171	–0.275
SC23													
1996	11.6m	305m	182m	124m	81.9m	26.9m	55.0m	98	54m	162	880/S,m	0.190	–0.343M
1997	28.9	686	432	254	208.6	111.5	97.1	111	94	140	1,000/S	0.259M	0.069
1998	88.3	1,937	914	1,023	760.8	335.5	425.3	143	134	152	1,460/S	–0.056	–0.118
1999	136.3	2,733	1,551	1,182	1,164.3	687.8	476.6	155	162	147	1,370/N	0.135	0.181
2000	173.9M	3,587M	1,822	1,765	1,609.7	829.7	780.0	164	167	162	2,140/N	0.016m	0.031
2001	170.4	3,476	1,863M	1,613	1,707.4	922.8M	784.6	179	181	178	2,440/N	0.072	0.081
2002	163.6	3,528	1,588	1,940M	1,833.8M	729.9	1,103.9M	190	168	208	1,990/S	–0.100	–0.204
2003	99.3	2,145	928	1,217	1,099.5	549.7	549.8	187	216	165	2,610/S,M	–0.135	–0.000m
2004	65.3	1,311	446	865	683.3	270.7	412.6	191	222M	175	2,010/N	–0.320	–0.208
2005	45.8	973	364	609	542.5	188.6	353.9	204M	189	212M	1,630/N	–0.252	–0.305
2006	24.7	600	114	486	245.0	19.8	225.2	149	63	169	750/S	–0.620	–0.838M
2007	12.6	308	58	250	134.4	12.3	122.1	159	77	178	540/S	–0.623M	–0.817
SC24													
2008	4.2m	122m	41m	81	22.9m	5.0m	17.8	69m	45m	80	300/S,m	–0.328	–0.559
2009	4.8	123	85	38m	26.1	18.1	7.9m	77	78	76m	380/N	0.382	0.391
2010	24.9	623	396	227	214.2	150.8	63.4	125	139	102	550/N	0.271	0.408
2011	80.8	1,788	1,194M	594	747.2	561.4M	185.8	153	172M	114	1,540/N	0.336	0.503
2012	84.5	1,848	965	883	798.6	405.9	392.8	158	154	163	1,460/S	0.044	0.016
2013	94.0	2,121	886	1,235	860.0	361.0	499.0	148	149	147	1,100/N	–0.165	–0.160
2014	113.3M	2,442M	894	1,548M	1,251.0M	310.2	940.8M	187M	127	222	2,750/S,M	–0.268	–0.504
2015	69.8	1,544	783	761	621.4	306.5	315.0	147	143	151	1,190/S	0.014m	–0.014m
2016	39.9	910	665	245	317.0	218.5	98.5	127	120	147	850/N	0.462	0.379
2017	21.7	477	343	134	217.5	133.5	84.0	166	142	229M	1,060/S	0.438	0.228
2018	7.0	161	94	67	24.4	12.7	11.7	55	49	64	240/S	0.168	0.041
2019	3.6	97	89	8	17.3	17.1	0.2	103	70	9	420/N	0.835M	0.977M
mean			873.3	852.7		425.0	412.5		157	154		0.009	0.020
sd			703.6	680.6		399.5	381.4		49	47		0.281	0.363
even cycles													
mean			803.2	795.7		386.6	383.9		153	148		0.019	0.045
sd			616.0	657.8		344.5	362.4		50	50		0.295	0.369
odd cycles													
mean			950.7	915.6		467.2	444.1		160	160		–0.004	–0.009
sd			786.6	704.4		451.4	401.6		50	44		0.265	0.345

Note: Asymmetry = (*N*–*S*)/*C*, where *C* is the combined total (=*N*+*S*)

@ means end of the RGO dataset.

The largest individual spot group was active region 1488603, having a corrected area spot size of 6,132 millionth of a solar hemisphere on 04/08/1947 and designated RGO type 8.

Table 2 provides a simple comparison of the timing occurrences of m and M for N and S parametric values with respect to the occurrences of SSN(m) and SSN(M), where the value '0' denotes that the parametric values occurred simultaneously (same year) with the corresponding SSN(m) and SSN(M) occurrences. Positive numbers indicate that the parametric values occurred (in years) after the corresponding SSN(m) and SSN(M) occurrences, while negative numbers indicate that the parametric values occurred (in years) before the corresponding SSN(m) and SSN(M) occurrences. Also given are the ascent (ASC) and descent (DES) intervals (in years) for each SC, where ASC is the time from to SSN(m) to SSN(M) for cycle *n*, while DES is the time from SSN(M) for cycle *n* to SSN(m) for cycle *n* + 1.

Table 2. Comparison of parametric m and M hemispheric occurrences with respect to corresponding occurrences of SSN(m) and SSN(M).

			SSA(N)		SSA(S)		NARE(N)		NARE(S)		MAE(N)		MAE(S)	
SC	ASC	DES	SSA (m)	SSA (M)	SSA (m)	SSA (M)	NARE (m)	NARE (M)	NARE (m)	NARE (M)	MAE (m)	MAE (M)	MAE (m)	MAE (M)
12	5	6	+1	–2	0	0	+1	–1	0	+1	+1	–3	0	0
13	4	8	0	–1	+1	0	0	0	+1	0	0	+3	–1	+4
14	4	8	0	0	0	+2	0	+1	0	+2	–1	0	0	+2
15	4	6	–1	0	0	0	–1	0	0	0	–1	+2	0	0
16	5	5	0	0	0	–1	0	0	0	–1	0	–2	0	–2
17	4	7	+1	0	0	+1	+1	0	0	+1	+1	+6	0	+1
18	3	7	0	+2	–1	0	0	+2	–1	0	0	–1	–1	0
19	3	7	0	+2	0	+1	0	+1	0	+2	0	+2	–1	+1
20	4	8	0	–1	0	2	0	–1	+1	–1	0	0	0	+3
21	3	7	–1	0	–1	+1	0	0	–1	0	–2	+3	–1	+2
22	3	7	0	0	0	+2	0	0	0	+2	+1	0	0	0
23	4	8	0	+1	0	+2	0	+1	0	+2	0	+4	–2	+2
24	6	≥4#	0	–3	+1	0	0	–3	+1	0	0	–3	+1	+3

Note: # means SC24 DES is unknown; assumes SC25 in 2019.

Figures 1–3 display the annual variations of (1) (a) SSA(N) and (b) SSA(S), (2) (a) NARE(N) and (b) NARE(S), and (3) (a) MAE(N) and (b) MAE(S), respectively. Across the top of figures 1 and 2 are identified the years when SSN(m) and SSN(M) occurred per SC (located along the bottom in fig. 3), where SSN(m) occurrences are shown as unfilled triangles and SSN(M) occurrences are shown as filled triangles. The data intervals are divided according to whether the values come from the RGO record (1875–1976) or the extended record based on the USAF/NOAA observations (1977–present). The horizontal line in each figure gives the overall mean (given to the right along with *sd*) for the interval 1875–2017 and the numbers SC12–SC24 refer to the specific SCs. Plainly, the years 2018/2019 represent transitional years between the ending of SC24 and the onset of SC25, which is anticipated to occur either in late 2019 or 2020,

based on smoothed monthly mean SSN (cf. Wilson 2019a, 2019b, 2020). (It is now known that SC25 minimums for SSN and SSA occurred in 2019.)

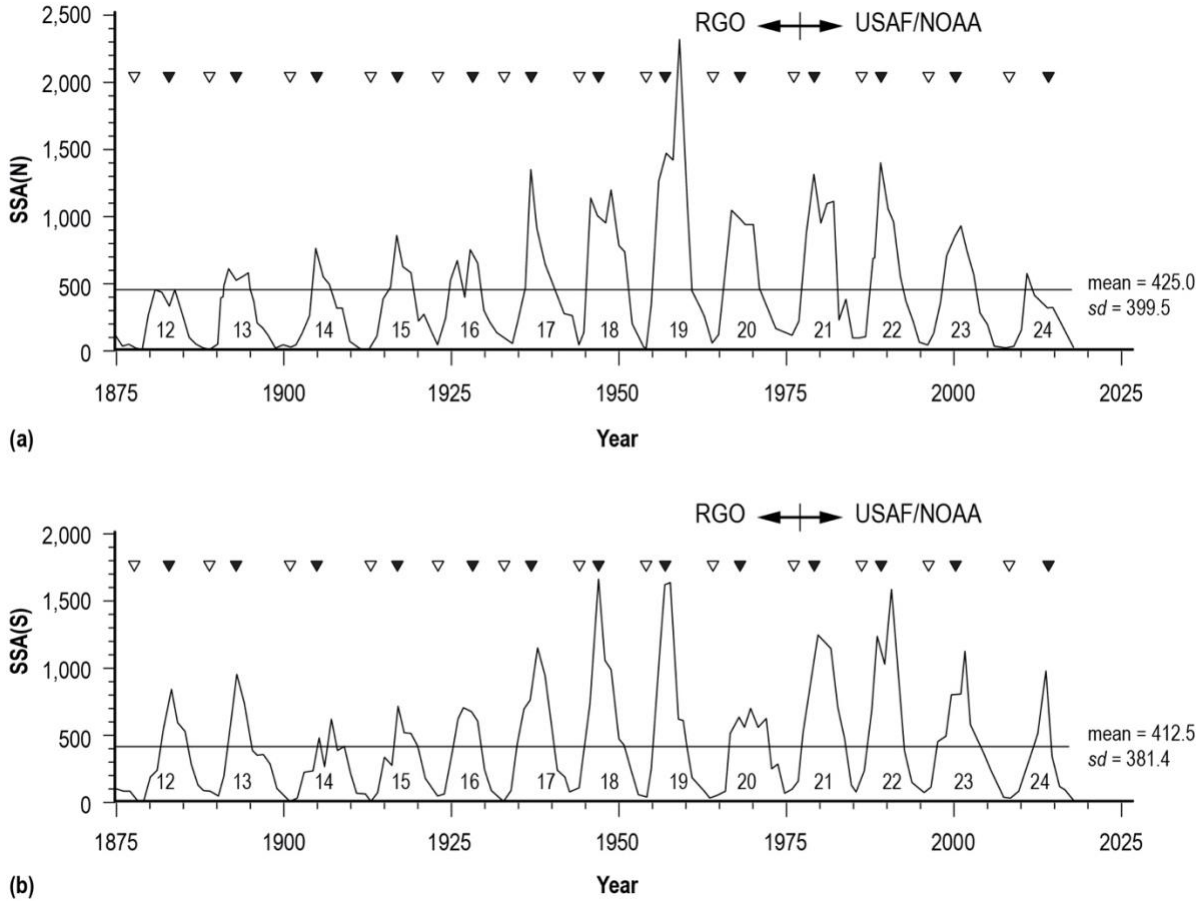

Figure 1. Annual variation of (a) SSA(N) and (b)SSA(S).

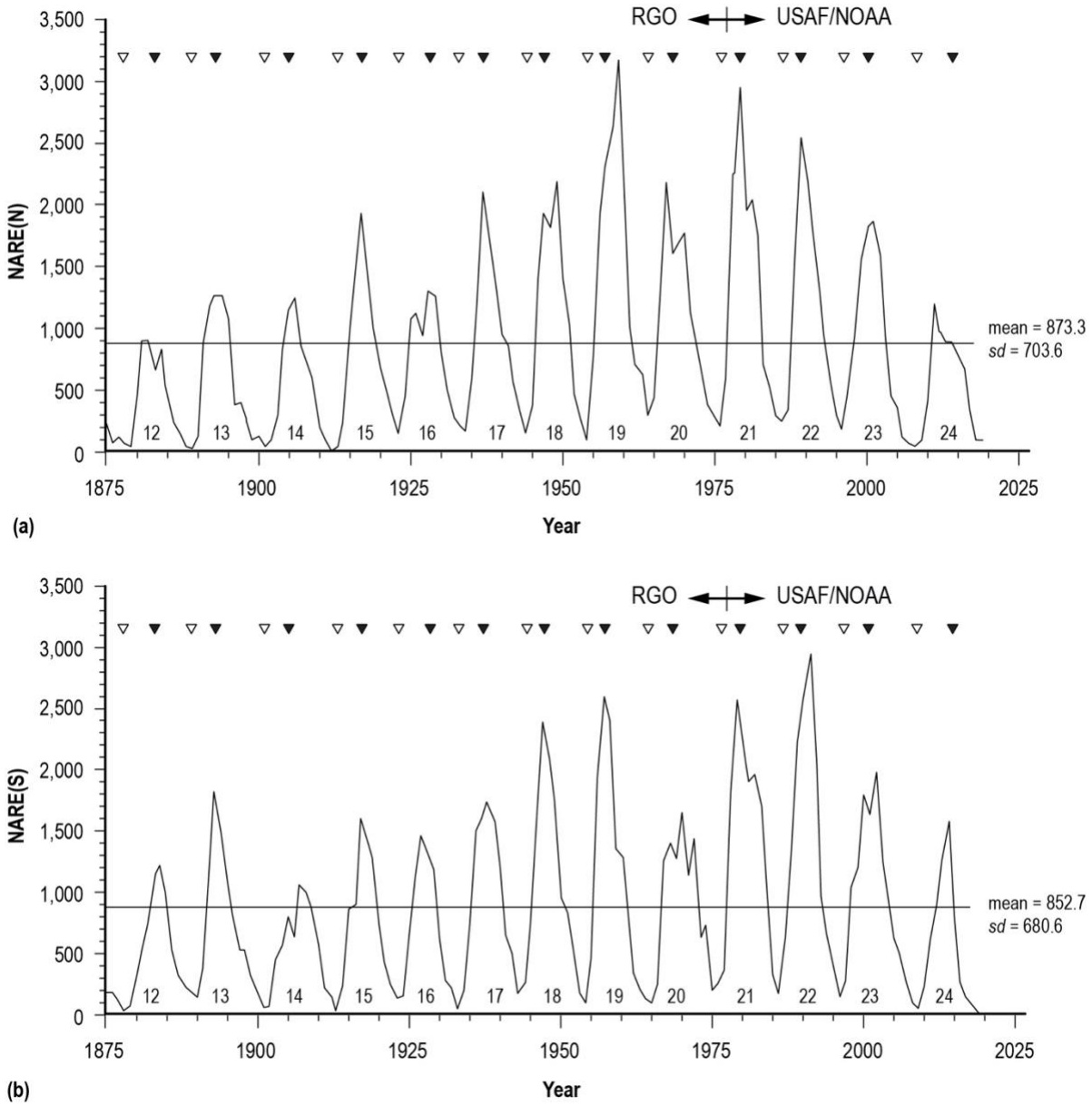

Figure 2. Annual variation of (a) NARE(N) and (b) NARE(S).

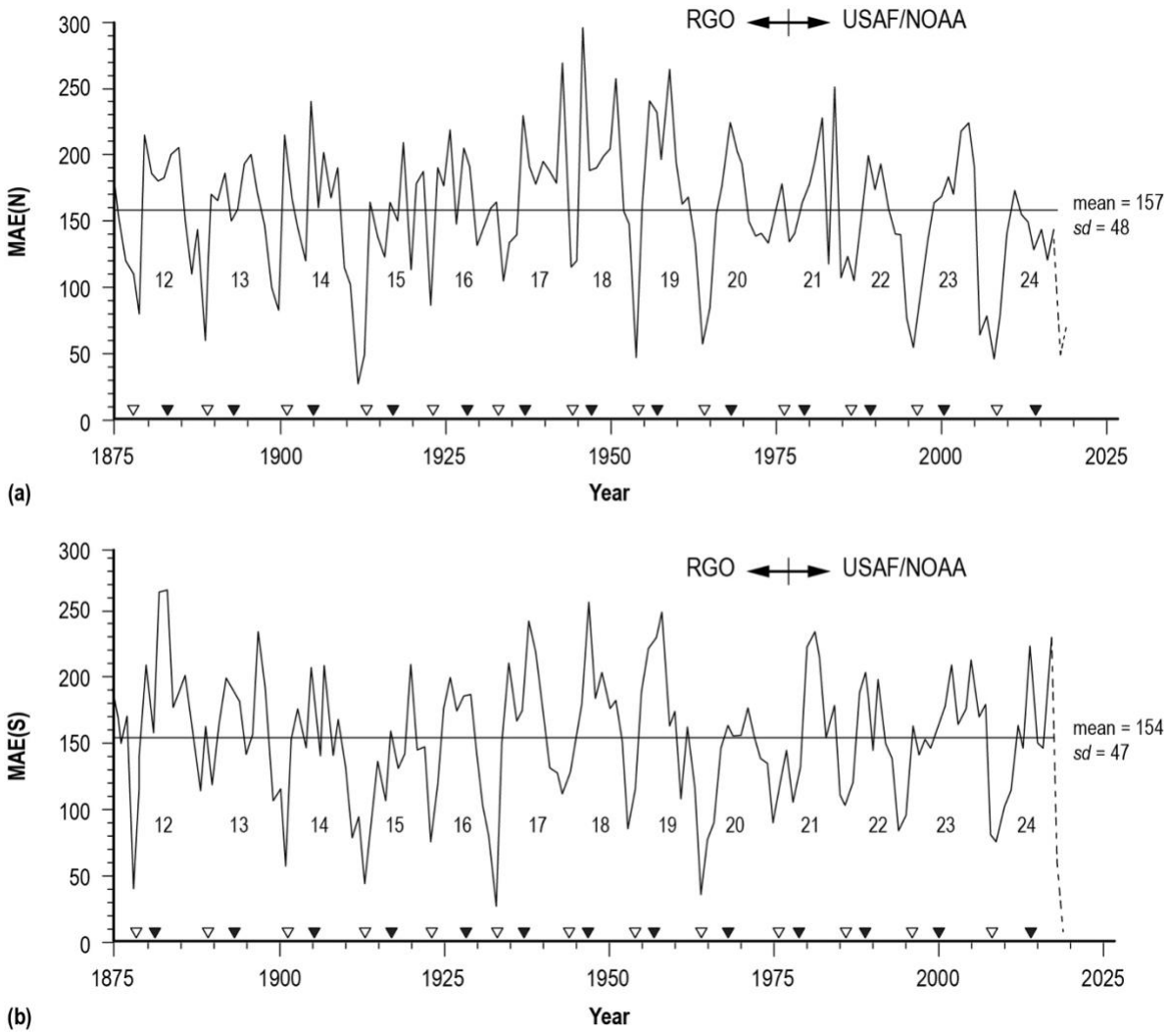

Figure 3. Annual variation of (a) MAE(N) and (b) MAE(S).

Figure 1a shows that the maximum in SSA(N) per SC increased between SC12 and SC19 and decreased between SC19 and SC24. SC19 had the largest yearly SSA(N), measuring 2,277.2 millionths of a solar hemisphere and occurring in 1959, some 2 years after SC19 SSN(M). The timing of the maximum for SSA(N) has occurred simultaneously with the maximum SSN(M) for only 6 of 13 SCs. For SC12, SC13, SC20, and SC24, maximum SSA(N) preceded SSN(M), while for SC18, SC19 and SC23, maximum SSA(N) followed SSN(M). Minimum SSA(N) nearly always has occurred simultaneously with SSN(m), with only SC12, 17, and 21, having minimum SSA(N) occurrences that differed by 1 year from SSN(m).

Figure 1b shows that the maximum in SSA(S) per SC also increased, especially, between SC14 and SC18–SC19 and decreased afterwards through SC24. The largest yearly SSA(S) measured 1,642.9 millionths of a solar hemisphere and occurred in 1947 (SC18), simultaneously with SC18 SSN(M). The timing of maximum in SSA(S) is found to have followed SSN(M) in 7 of 13 SCs, occurring simultaneously in 5 of 13 SCs and preceded by one year only in SC16. Like SSA (N), the minimum in SSA(S) usually occurs simultaneously with SSN(m), with only SC14,

SC16, SC17, and SC21 having minimum SSA(S) occurrences that differed by one year from SSN(m).

Comparing the minimums of SSA(N) and SSA(S), they occurred simultaneously in 7 of 13 SCs, including SC14, SC16 and SC19–SC23. Comparing the maximums of SSA(N) and SSA(S), they have occurred simultaneously in only 1 of 13 SCs (SC15). The maximum SSA(S) usually occurs after the maximum SSA(N), true for 9 of 13 SCs. For SC16, SC18, and SC19, the maximum SSA(S) occurred earlier than the maximum SSA(N). The mean SSA(N) measures 425.0 millionths of a solar hemisphere (*sd* = 399.5 millionths of a solar hemisphere), while the mean SSA(S) measures 412.5 millionths of a solar hemisphere (*sd* = 381.4 millionths of a solar hemisphere); hence, there is no statistically significant difference in the hemispheric means based on SSA.

Interesting is that many SCs have multiple peaks in SSA(N) and SSA(S), typically 2–3 years apart. Such behavior is clearly seen in SC12, SC13, SC16, SC18, SC19, and SC21 in SSA(N) and SC14, SC15, SC20, and SC22 in SSA(S). The rankings of maximum SSA(N) from least to greatest are as follows: SC12 (452.0); SC24 (561.4); SC13 (602.0); SC16 (725.9); SC14 (749.3); SC15 (853.6); SC23 (922.8); SC20 (1033.6); SC18 (1,180.2); SC21 (1,289.9); SC17 (1,316.1); SC22 (1,363.8); and SC19 (2,277.2). The rankings of maximum SSA(S) from least to greatest are as follows: SC14 (600.3); SC15 (680.4); SC16 (681.9); SC20 (683.3); SC12 (820.9); SC24 (940.8); SC13 (944.0); SC23 (1,103.9); SC17 (1,129.2); SC21(1,227.1); SC22 (1,555.8); SC19 (1,608.8) and SC18 (1,642.9). On average, the maximum SSA(N) measures 1,025.2 millionths of a solar hemisphere (*sd* = 482.1) and the maximum SSA(S) measures 1,047.6 millionths of a solar hemisphere (*sd* = 370.2). The average time from minimum to maximum SSA(N) is 3.8 years (range 2–5 years), while the average time from minimum to maximum SSA(S) is 4.8 years (range 3–6 years). The average time from maximum to minimum SSA(N) is 6.9 years (range 5–9 years), while the average time from maximum to minimum SSA(S) is 6.2 years (range 5–8 years). For SC24, the elapsed time from its maximum to minimum SSA(N) for SC25 measures at least 6 years (if 2018 marks the occurrence of the minimum of SSA(N) for SC25), while the elapsed time from maximum to minimum SSA(S) for SC25 measures, at least 5 years (presuming 2019 marks the occurrence of minimum SSA(S) for SC25).

Figure 2 shows the yearly hemispheric variation of NARE, following the same format used in figure 1. Regarding figure 2a, it shows that the maximum in NARE(N) per SC increased between SC12 and SC19 and decreased between SC19 and SC24, as it occurred with SSA(N). SC19 had the largest yearly NARE(N), numbering 3,173 entries and occurring in 1959, some 2 years after SC19 SSN(M), as also was seen for SSA(N). The timing of the maximum for NARE(N) has occurred simultaneously with SSN(M) for only 6 of 13 SCs. For SC12, SC20, and SC24, the timing of maximum NARE(N) preceded SSN(M), while for SC18, SC19, and SC23, maximum NARE(N) followed SSN(M). Minimum NARE(N) nearly always has occurred simultaneously with SSN(m), with only SC12, 15, and 17 having minimum NARE(N) occurrences that differed by one year from SSN(m). Regarding figure 2b, it shows that the maximum in NARE(S) per SC also increased, especially, between SC14 and SC18–SC22 and decreased afterwards through SC24. The largest yearly NARE(S) numbered 2,917 entries and occurred in 1991 (SC22). The timing of the maximum of NARE(S) is found to have followed SSN(M) in 6 of 13 SCs, occurred simultaneously in 5 of 13 SCs and preceded by one year only in SC16 and 20. Like NARE(N), the minimum in NARE(S) usually occurs simultaneously with SSN(m), with only SC12, SC15, and SC17 having minimum NARE(S) occurrences that differed by one year from SSN(m).

Comparing the minimums of NARE(N) and NARE(S), they occurred simultaneously in 5 of 13 SCs, including SC14, SC16, SC19, SC22, and SC23. Comparing maximums of NARE(N) and NARE(S), they have occurred simultaneously in only 4 of 13 SCs, including SC13, SC15, SC20, and SC21. The maximum NARE(S) usually occurs after the maximum NARE(N), true for 7 of 13 SCs, including SC12, SC14, SC17, SC19, and SC22–SC24. For SC16 and SC18, the maximum NARE(S) occurred earlier than the maximum NARE(N). The mean NARE(N) measures 873.3 entries (*sd* = 703.6), while the mean NARE(S) measures 852.7 entries (*sd* = 680.6); hence, as with SSA, there is no statistically significant difference in the hemispheric means of NARE.

Double-peaking is found to have occurred in SC12, SC16, SC18, SC20 and SC21 for NARE(N) and in SC14, SC20, SC21 and SC23 for NARE(S), typically 2 years apart. The rankings of maximum NARE(N) from least to greatest are as follows: SC12 (895), SC24 (1,194), SC14 (1,235), SC13 (1,264), SC16 (1,301), SC23 (1,863), SC15 (1,938), SC17 (2,114), SC20 (2,159), SC18 (2,177), SC22 (2,532), SC21 (2,904) and SC19 (3,173). The rankings of maximum NARE(S) from least to greatest are is as follows: SC14 (1,053), SC12 (1,206), SC24 (1,251), SC16 (1,428), SC15 (1,572), SC20 (1,622), SC17 (1,711), SC13 (1,808), SC23 (1,940), SC18 (2,368), SC21 (2,534), SC19 (2,560) and SC22 (2,917). On average, the maximum NARE(N) numbers 1,903.8 entries (*sd* = 703.2), while on average, the maximum NARE(S) numbers 1,843.8 entries (*sd* = 586.2). The average time from minimum to maximum NARE(N) is 4.0 years (range 3–5 years), while the average for NARE(S) is 4.6 years (range 3–6 years). For NARE(N), six SCs had intervals of rise (minimum to maximum) of 3 years, including SC12, SC17, SC20–SC22, and SC24, while six SCs had intervals of rise of 5 years, including SC14–SC16, SC18, SC19, and SC23. For NARE(S), four SCs had intervals of rise of 4 years, including SC15, SC16, SC18, and SC21, while, four SCs had intervals of rise of 5 years, including SC17, SC20, SC22, and SC24 and three SCs had intervals of rise of six years, including SC12, SC14, and SC23. (Obviously, strong linear correlations exist between SSN, SSA, and NARE.)

Figure 3 shows the yearly hemispheric variation of MAE. For both hemispheres, MAE appears to have multiple peaks. Also, there appears to be a downward trend in MAE for both hemispheres between SC12 and SC15, followed by an upward trend between SC15 and SC18/19 and another downward trend between SC18/19 and SC24, one that is more pronounced in the N hemisphere than in the S hemisphere. The means for the two hemispheres are not statistically different.

A comparison of the minimum MAE(N) with SSN(m) (see table 2) reveals that 7 of 13 SCs had simultaneous occurrences (i.e., no lag), 3 had minimum MAE(N) prior (1–2 years) to SSN(m), and 3 had minimum MAE(N) after (+1 year) SSN(m). A comparison of minimum MAE(S) with SSN(m) reveals that 8 of 13 SCs had simultaneous occurrences, 4 had minimum MAE(S) prior (1–2 years) to SSN(m), and 1 (SC24) had minimum MAE(S) after (+l year) SSN(m). Minimum MAE(N) and MAE(S) for SC25 may have occurred, respectively, in 2018 and 2019. Hence, SSN(m) for SC25 should be expected sometime about 2016–2019 based on the minimum occurrence of MAE(N) and about 2017–2020 based on the minimum occurrence of MAE(S). In terms of SSN, it decreased in value between 2016 and 2019, measuring 39.9 in 2016, 7.0 in 2018, and 3.6 in 2019. Clearly, SSN(m) for SC25 is near, expected to occur either in 2019 or 2020. (SSN(m) for SC25 occurred in 2019.)

The rankings from least to greatest maximum MAE(N) are as follows: SC24 (187), SC22 (197), SC13 (199), SC15 (208), SC12 (213), SC16 (218), SC20 (222), SC23 (222), SC14 (239), SC21 (249), SC19 (262), SC17 (267), and SC19 (293). In terms of rankings from least to greatest

maximum MAE(S), it is as follows: SC20 (176), SC16 (199), SC22 (200), SC14 (208), SC15 (209), SC23 (212), SC24 (229), SC21 (231), SC13 (235), SC17 (241), SC19 (246), SC18 (253) and SC12 (265). The maximum MAE(N) tends to occur before the maximum MAE(S), true for 8 of 13 SCs. On average, the maximum MAE(N) measures 229 millionths of a solar hemisphere (*sd* = 31 millionths of a solar hemisphere), and the maximum MAE(S) measures 223 millionths of a solar hemisphere (*sd* = 25 millionths of a solar hemisphere).

Figure 4 depicts the yearly variations of the asymmetry based on NARE (top) and SSA (bottom). Asymmetric values near zero simply mean that both hemispheres are approximately of equal parametric magnitude, whereas asymmetric values of large magnitude indicate that one hemisphere is of greater parametric magnitude than the other hemisphere. The greatest positive or negative asymmetric values tend to occur near SSN(m). For Asymmetry (NARE), the maximum asymmetric value has occurred –3 to +1 years relative to SSN(m) occurrence. For Asymmetry (SSA), the maximum asymmetric value has occurred –3 to +2 years relative to SSN(m) occurrence. Large positive asymmetric values (the largest on record) occurred in 2019 for both NARE and SSA. Hence, one expects SSN(m) for SC25 to very probably occur very soon (i.e., sometime between 2019 and 2022, assuming the year 2019 marks the greatest asymmetric value year). For 11 of 13 SCs, maximum Asymmetry (SSA), ignoring sign, occurs either simultaneously with SSN(m) (SC12, SC13, SC17, and SC23) or before SSN(m)(SC14, SC15, SC18, SC19, SC21, SC22, and SC24).

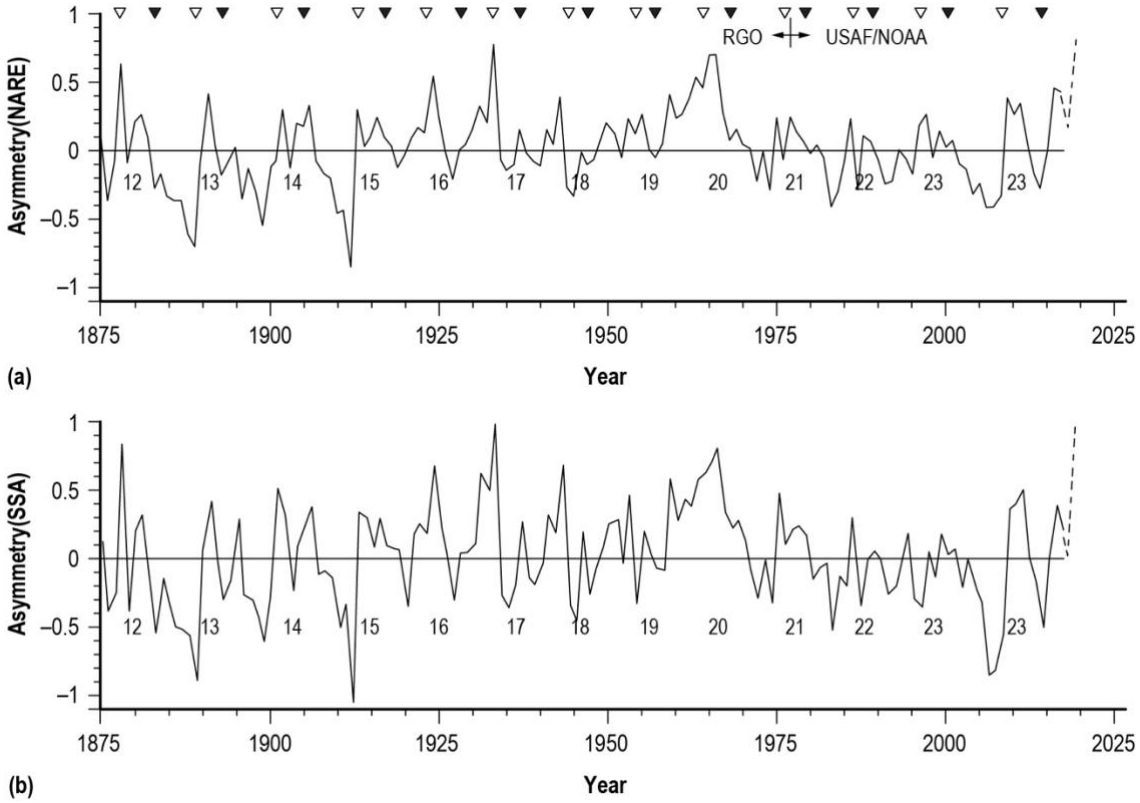

Figure 4. Annual variation of (a) Asymmetry(NARE) and (b) NARE(SSA).

Table 3 gives the parametric m and M values and the mean and *sd* values for SC12–SC24 and for even- and odd-numbered cycles (SC24 values are incomplete). Figure 5 depicts the m parametric cyclic variations (top) for SC12–SC25 and the M parametric variations (bottom) for SC1–SC24 (i.e., using the combined hemispheres). Figure 6 shows the m (top) and M (bottom) parametric cyclic hemispheric variations for SC12–SC25 and SC12–SC24, respectively. The downward pointing arrows in figures 5 and 6 denote that the true m values for SC25 could be smaller than shown, especially if SSN(m) for SC25 occurs in 2020 or later. The largest parametric m values occurred in SC21 (fig. 5), while the largest parametric M values occurred (fig. 5) in SC18 (MAE), SC19 (SSN and SSA) and SC21 (NARE). The largest m value based on N hemispheric values occurred (fig. 6) in SC21 (SSA and MAE) and SC20 (NARE), while the largest m value based on southern hemispheric values occurred in SC23 (SSA), SC21 (NARE) and SC18 (MAE). The largest M values based on northern hemispheric values (Figure 6) occurred in SC19 (SSA and NARE) and SC18 (MAE), while the largest M values based on southern hemispheric values occurred in SC18 (SSA), SC22 (NARE) and SC12 (MAE).

Table 3. Parametric m and M values.

	SSN		SSA		NARE		MAE		SSA(N)		SSA(S)		NARE(N)		NARE(S)		MAE(N)		MAE(S)	
Cycle	m	M	m	M	m	M	m	M	m	M	m	M	m	M	n	M	n	M	n	M
12	5.7	106.1	22.2	1,148.9	81	2,039	100	234	11.9	452.0	1.7	820.9	53	895	15	1,206	82	213	41	265
13	10.4	142.0	76.7	1,460.6	191	3,072	121	207	4.7	602.0	45.4	944.0	29	1,264	142	1,808	59	199	116	235
14	4.6	105.5	27.9	1,195.9	78	1,951	100	225	21.2	749.3	6.6	600.3	36	1,235	42	1,053	82	239	57	208
15	2.4	173.6	7.5	1,533.9	60	3,510	46	171	0.8	853.6	2.5	680.4	11	1,938	21	1,572	27	208	43	158
16	9.7	129.7	54.7	1,388.9	244	2,613	82	209	32.6	725.9	22.0	681.9	138	1,301	106	1,428	86	218	76	199
17	9.2	190.6	91.3	2,072.8	225	3,705	127	219	44.3	1,316.1	1.8	1,129.2	156	2,114	25	1,711	104	267	26	241
18	16.1	214.7	124.7	2,634.1	370	4,298	123	235	42.2	1,180.2	45.9	1,642.9	135	2,177	152	2,368	114	293	110	253
19	6.6	269.3	34.6	3,048.5	166	5,016	76	232	11.7	2,277.2	22.9	1,608.8	93	3,173	73	2,560	46	262	86	246
20	15.0	150.0	53.9	1,601.3	390	3,390	51	194	44.1	1,033.6	9.8	683.3	284	2,159	77	1,622	57	222	34	176
21	18.4	220.1	166.4	2,270.2	426	5,438	128	220	95.0	1,289.9	44.5	1,227.1	198	2,904	183	2,534	131	249	89	231
22	14.8	211.1	123.2	2,572.0	394	4,751	108	198	80.4	1,363.8	42.8	1,555.8	242	2,532	152	2,917	104	197	103	200
23	11.6	173.9	81.9	1,833.8	305	3,587	87	204	26.9	922.8	55.0	1,103.9	182	1,863	124	1,940	54	222	84	208
24	4.2	113.3	22.9	1,251.0	122	2,442	69	187	5.0	561.4	7.9	940.8	41	1,194	38	1,548	45	172	76	229
mean	9.9	169.2	68.3	1,847.1	235	3,524	94	210	32.4	1,025.2	23.8	1,047.6	123	1,904	88	1,867	76	228	72	219
sd	5.1	50.6	48.0	619.3	132	1,116	28	20	29.0	482.1	20.2	370.2	88	703	58	567	31	33	30	31
Even(7)																				
mean	10.0	147.2	61.4	1,684.6	240	3,069	90	212	33.9	866.6	14.1	989.4	133	1642	83	1,735	81	222	71	219
sd	5.3	47.5	44.8	645.1	146	1,107	25	20	25.2	334.7	15.4	431.7	99	631	55	669	24	38	29	32
Odd(6)																				
mean	9.8	194.9	76.4	2,036.6	229	4,055	98	209	30.6	1,210.3	28.7	1,115.6	112	2209	95	2,021	70	235	74	220
sd	5.3	44.5	54.5	584.0	125	942	33	21	35.4	589.2	23.1	308.2	80	708	66	425	39	29	33	33

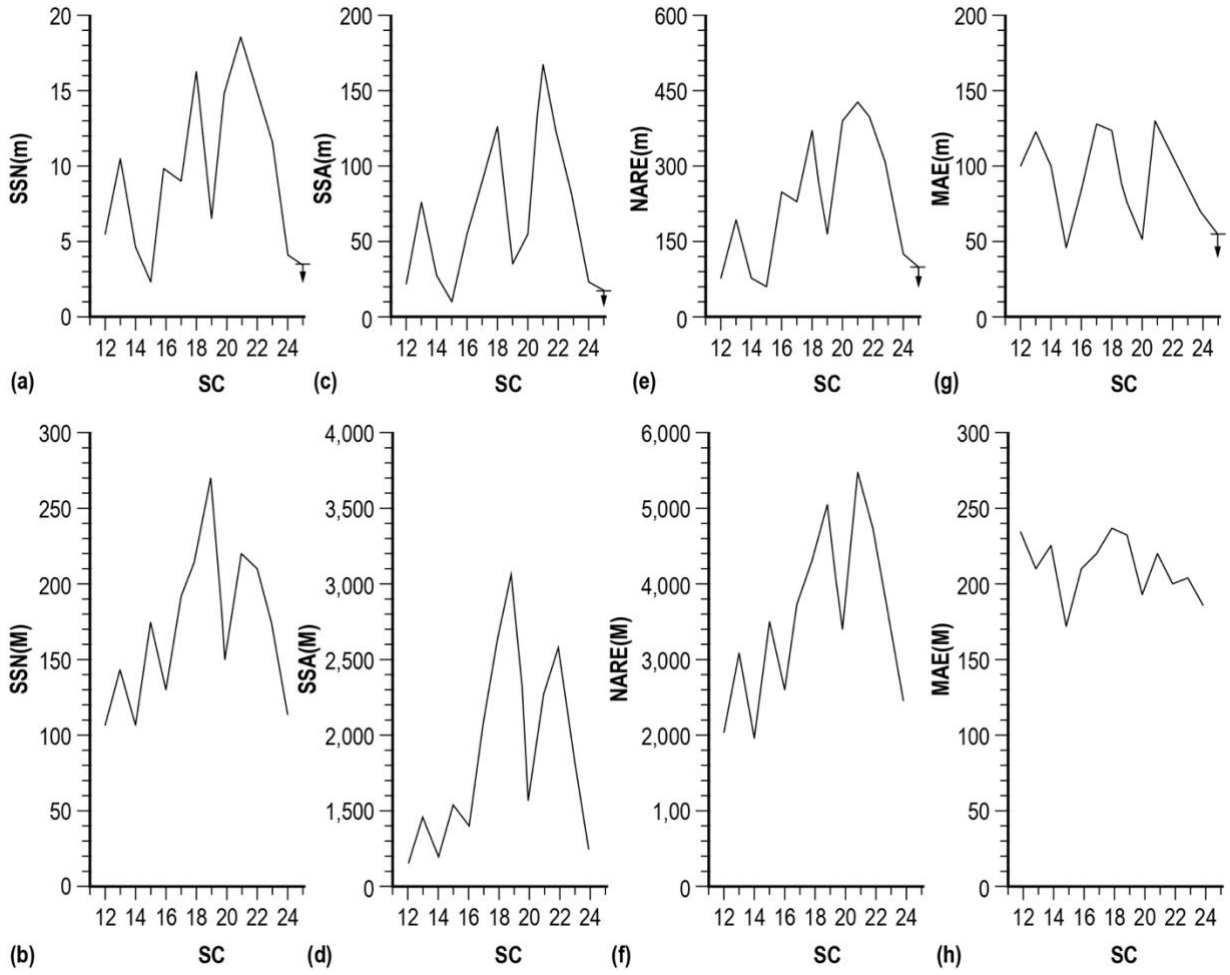

Figure 5. Cyclic variation of (a) SSN(m), (b) SSN(M), (c) SSA(m), (d) SSA(M), (e) NARE (m), (f) NARE(M), (g) MAE(m), and (h) MAE(M).

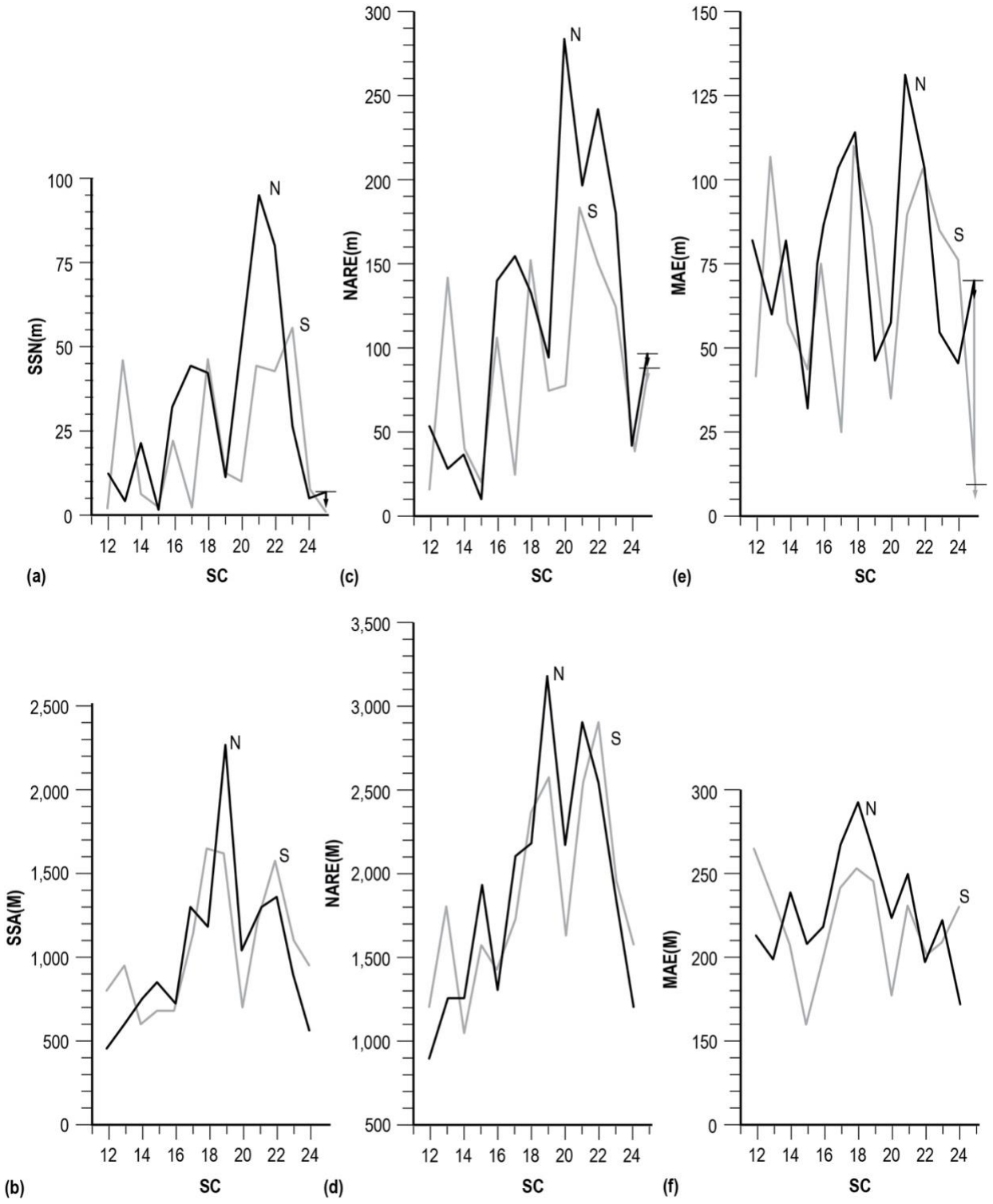

Figure 6. N-S cyclic variation of (a) SSA(m), (b) SSA(M), (c) NARE(m), (d) NARE(M), (e) MAE(m), and (f) MAE(M).

Figure 7 displays the parametric variations based on SC12–SC23 relative to SSN(m) for (a) SSA, (b) NARE, and (c) MAE. In the figure, the thicker darker line represents the northern hemispheric parametric mean; the thinner lighter line represents the southern parametric mean; the darker dotted line (filled circles) represents SC24 northern hemispheric values; and the lighter dotted line (unfilled circles) represents SC24 southern hemispheric values. Marked across the top are the SSN(M) occurrences for SC12–SC24. The t = 10 values for SC24 correspond to the yearly 2018 values (see table 1; the yearly 2019 values are lower still for SSN, SSA, SSA(S), MAE(S), NARE, NARE(N) and NARE(S)). Interesting is the behavior of SSA(N), NARE(N), and MAE(N) near SSN(m) for SC24. Comparison of the 2018 yearly values to values in 2006–2008 are suggestive that SC25(m) should be expected to occur within two years following 2018 (i.e., 2019 or 2020).

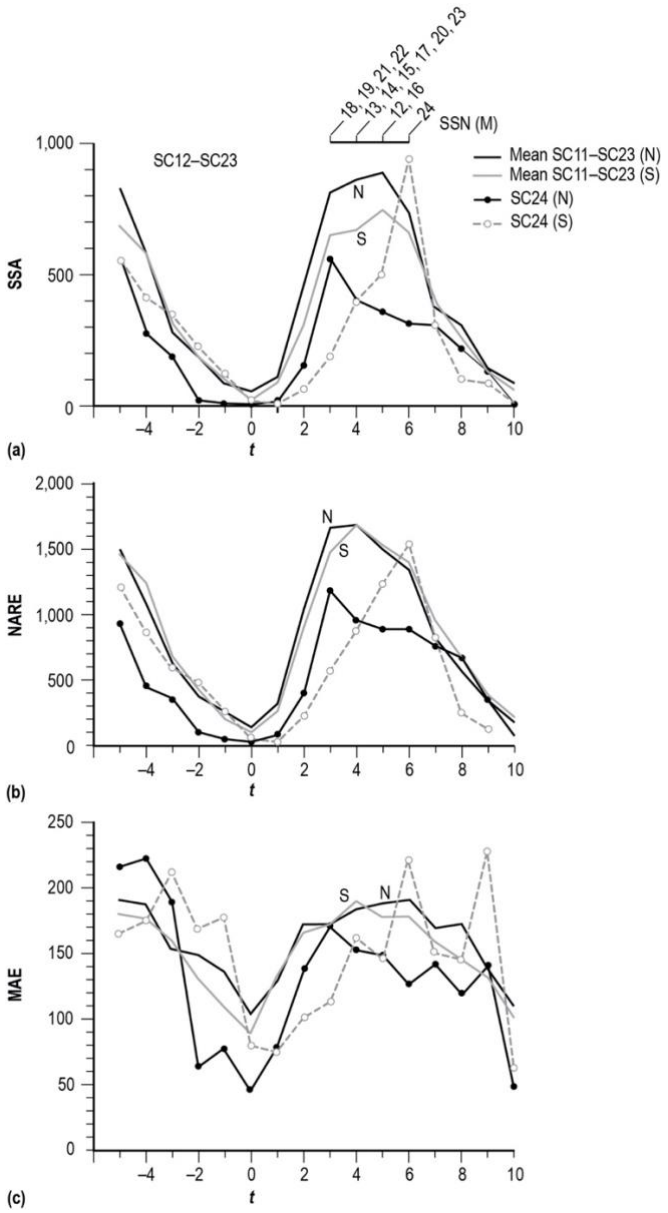

Figure 7. N-S variation of mean SC12–SC23 and annual SC24 values relative to SSN(m) for (a) SSA, (b) NARE and (c) MAE, for elapsed time *t* (in years) equal to –5 to +10.

Figure 8 is similar to figure 7 but now is plotted in terms of even- and odd-numbered SCs. For the odd-numbered SC, the plotted SC24 values presume SSN(m) for SC25 in 2019. If it turns out that the year 2020 marks the true occurrence of SSN(m) for SC25, then the plotted points must be shifted one year earlier (i.e., to the left). (SSN(m) for SC25 occurred in 2019.)

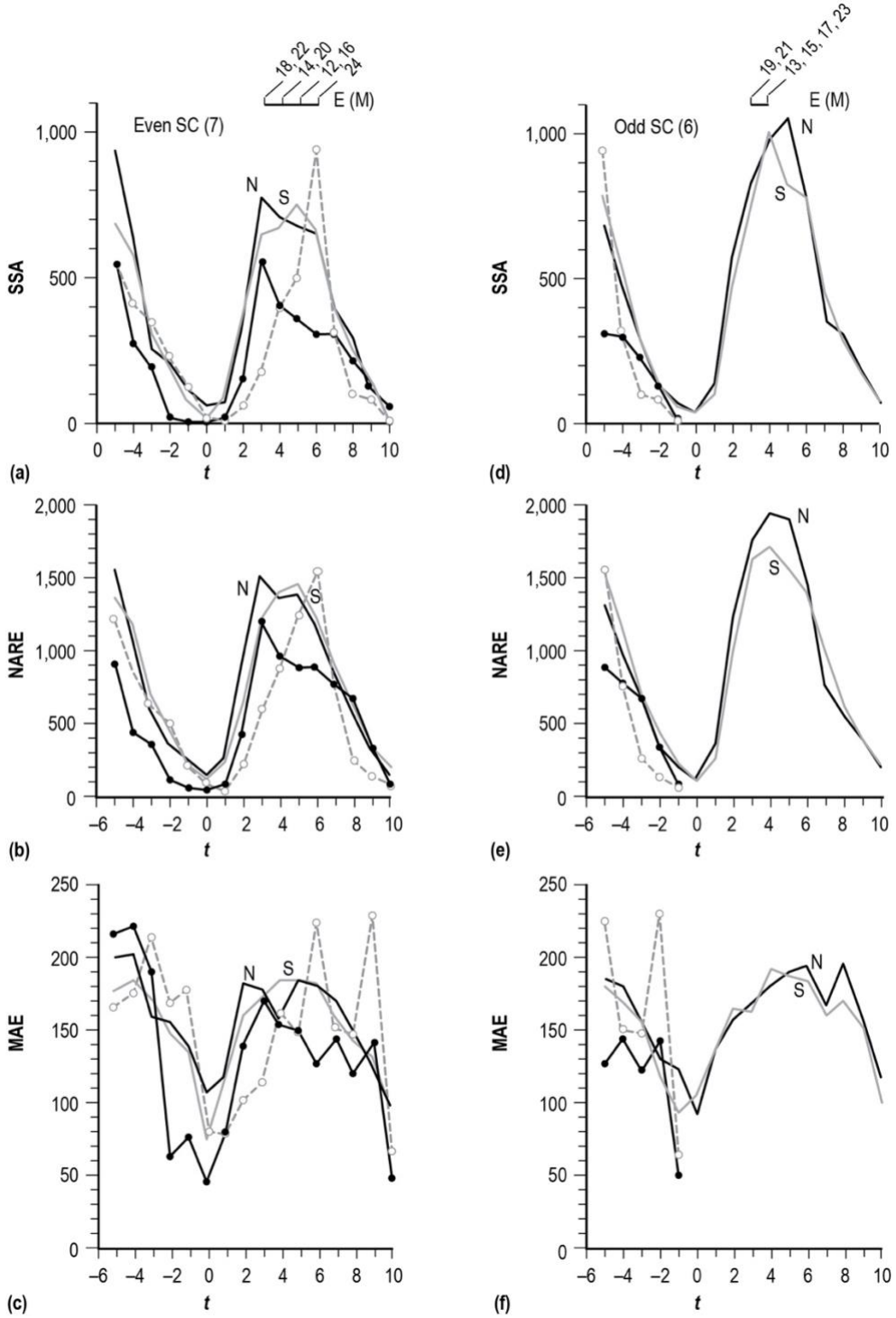

Figure 8. N-S variation of mean even- and odd-numbered SC and annual SC24 values relative to SSN(m) for (a) SSA, (b) NARE and (c) MAE, for elapsed time *t* (in years) equal to –5 to +10.

Figure 9 plots Asymmetry(SSA) and Asymmetry(NARE). Again, SC24 values are plotted assuming SSN(m) for SC25 occurred in 2019. The greatest negative Asymmetry(SSA) for SC24 occurred at $t = -2$ (2006), while the greatest positive Asymmetry(SSA) for SC24 appears to have occurred at $t = 11$ (2019, not shown; see table 1), surpassing the value at $t = +3$ (2011).

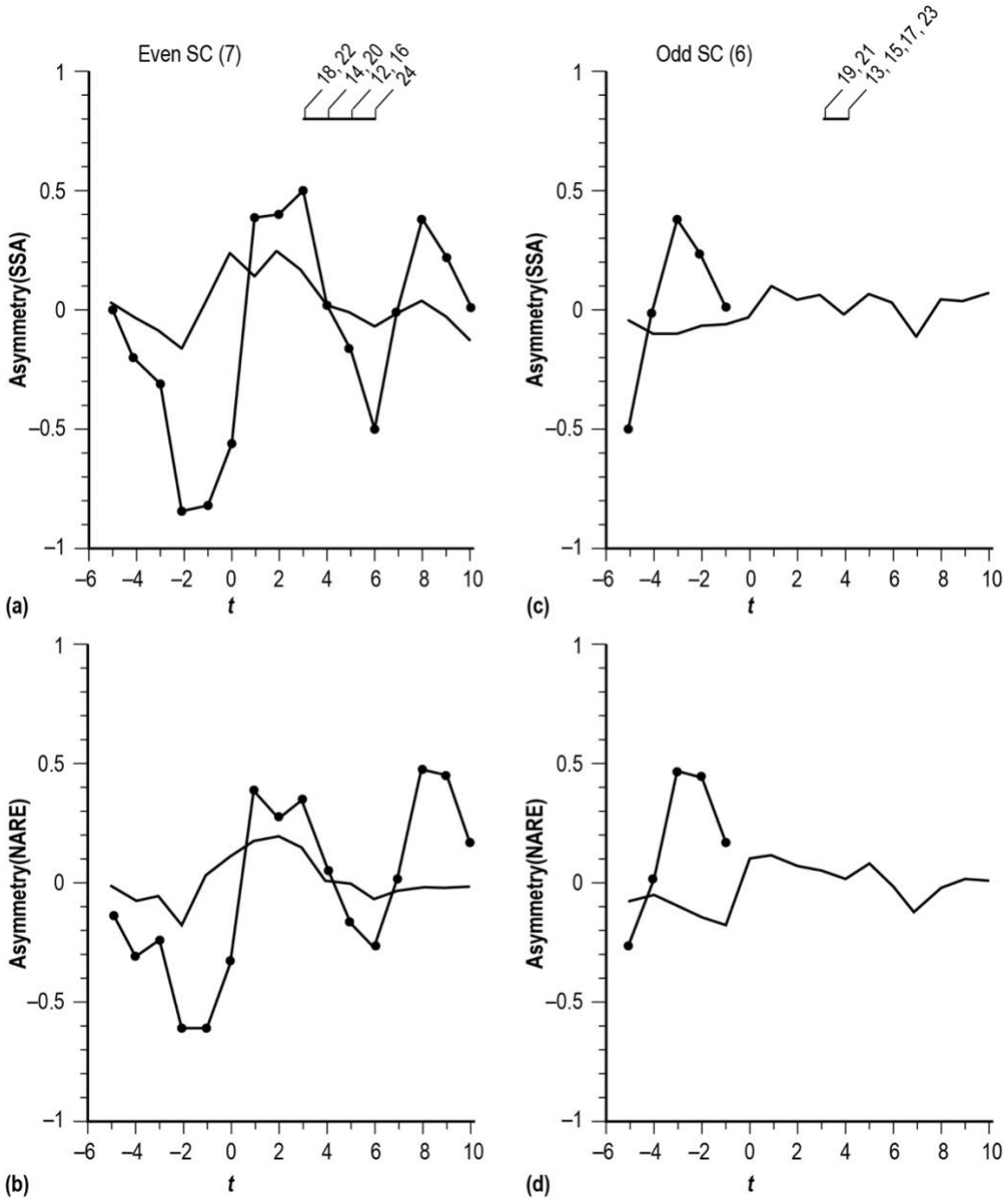

Figure 9. Variation of Asymmetry of mean of even- and odd-numbered SC and annual SC24 values relative to SSN(m) for (a) SSA and (b) NARE, for elapsed time *t* (in years) equal to –5 to +10.

Figure 10 simply shows the cyclic variation of LAAR/H. The northern hemisphere had the largest spots at minimum (m) in SC12, SC14–SC17, and SC21 and the largest spots at maximum (M) in SC12, SC16, SC17 and SC19–SC22. For SC24 the S hemisphere had the largest LAAR/H at both m and M. The largest LAAR/H at maximum occurred in SC18 in 1947 (SC18), measuring 6,132 millionths of a solar hemisphere, while the LAAR/H at minimum occurred in 1934 (SC17), measuring 1,169 millionths of a solar hemisphere.

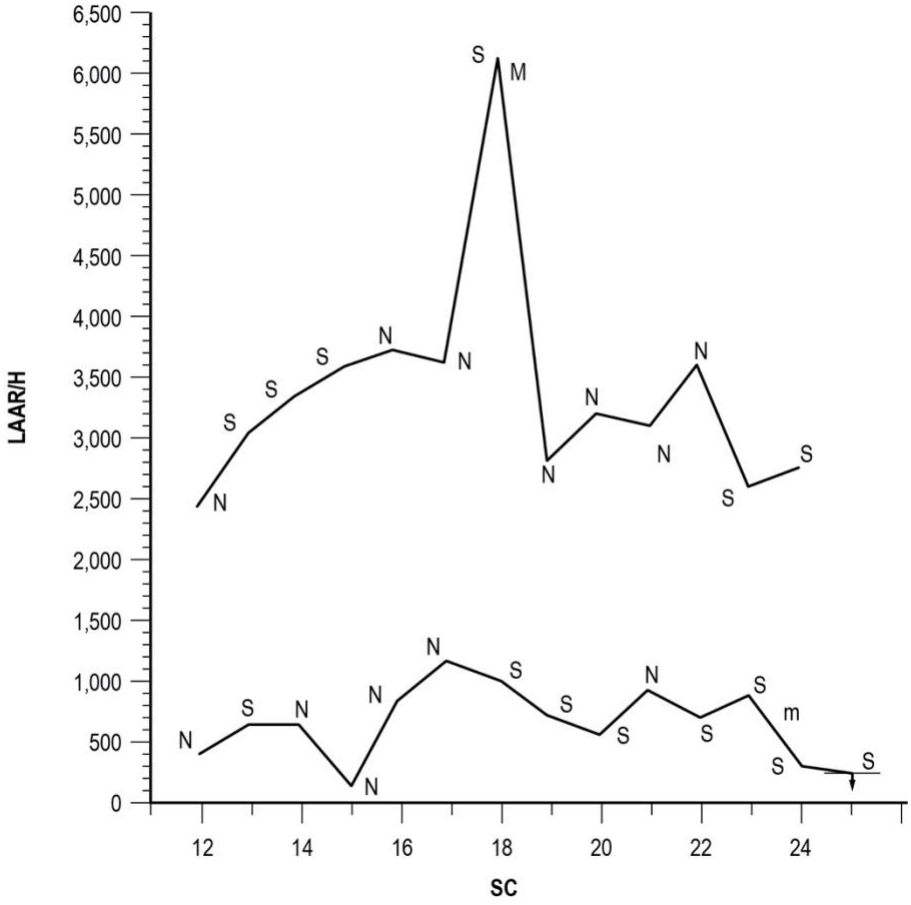

Figure 10. Cyclic variation of minimum and maximum LAAR/H.

Table 4 summarizes the behavioral dominance (i.e., number of years) of the N-S SSA per SC, both in terms of the overall SC and the ASC and DES intervals. For SC12–SC24, SSA(N) was larger than SSA(S), 75 versus 66 years. During the ASC interval, SSA(N) likewise, has been the more dominant, 35 versus 17 years, while during the DES interval, SSA(S) has been the more dominant, 49 versus 40 years. For even-numbered SCs, SSA(N) has been the more dominant overall and during the ASC interval, 43 versus 33 years, and 21 versus 9 years, respectively, while for odd-numbered SCs, SSA(S) has been the more dominant during the DES interval, 25 versus 18 years, while being less dominant during the ASC interval, 8 versus 14 years.

Table 4. N-S SSA dominance per SC.

	Overall		ASC		DES	
Cycle	N	S	N	S	N	S
12	3	8	3	2	0	6
13	3	9	2	2	1	7
14	5	7	3	1	2	6
15	9	1	4	0	5	1
16	9	1	4	1	5	0
17	5	6	1	3	4	3
18	5	5	1	2	4	3
19	7	3	2	1	5	2
20	8	4	4	0	4	4
21	4	6	3	0	1	6
22	6	4	2	1	4	3
23	4	8	2	2	2	6
24#	≥7	≥4	4	2	≥3	≥2
Total#	≥75	≥66	35	17	≥40	≥49
Even#	≥43	≥33	21	9	≥22	≥24
odd	32	33	14	8	18	25

Note: # means SC24 DES is unknown; excludes values for 2019.

In conclusion, this study has examined the N-S yearly variations of SSA, NARE, and MAE. For the overall interval of 1875–2019, the northern hemisphere has been the more dominant hemisphere in 77 of 145 years based on SSA. Likewise, for SC12–SC24, SSA(N) has been greater than SSA(S) during the ascending phase of the solar cycle (i.e., 35 of 52 years), whether the SC is an even- or odd-numbered SC, while SSA(S) has been greater than SSA(N) during the descending phase of the solar cycle (51 of 93 years). Minimum SSA(N) and SSA(S) have occurred in the same year in only 7 of 13 SCs including SC14, SC16, and SC19–SC23. Maximum SSA(N) and SSA(S) have occurred in the same year only once (in SC15). Maximum SSA(S) usually occurs after maximum SSA(N), true for 9 of 13 SCs. Maximum SSA(S) preceded maximum SSA(N) in SC16, SC18 and SC19. Multiple peaks in SSA(N) or SSA(S), typically 2–3 years apart, have often been seen (e.g., SC12–SC16 and SC18–SC22). SC12 had the smallest maximum SSA(N) (452.0 millionths of a solar hemisphere), while SC19 had the largest maximum SSA(N) (2,277.2 millionths of a solar hemisphere). SC14 had the smallest SSA(S) (600.3 millionths of a solar hemisphere), while SC18 had the largest SSA(S) (1,642.9 millionths of a solar hemisphere). The average time from minimum to maximum SSA(N) is 3.8 years (range 2–5 years), while it is 4.8 years for SSA(S) (range 3–6 years). The average time from maximum SSA(N) to the following minimum SSA(N) is 6.9 years (range 5–9 years), while it is 6.2 years for SSA(S) (range 5–8 years). The largest N-S asymmetry coefficients for SSA occurs between –3 and +1 year about sunspot minimum. The largest N-S asymmetry coefficient in SSA occurred in 2019 (SC24). The largest area sunspot occurred in 1947 (SC18), occurring in the southern hemisphere and measuring 6,132 millionths of a solar hemisphere, nearly twice the size of the average maxima of the largest area spots in the other 12 SCs. SSA and NARE are highly correlated with each other and with SSN. Minimum MAE(N) and MAE(S) may have occurred, respectively, in 2018 and 2019, highly suggestive that SSN(m) for SC25 either occurred in 2019 or will occur in 2020. (SSN(m) for SC25 is now known to have occurred in 2019.)

LITERATURE CITED

Antalová, A. and M. N. Gnevyshev 1983. Latitudinal Distribution of Sunspot Areas during the Period 1874–1976, *Contributions of the Astronomical Observatory Skalnate Pleso*, 11, pp. 63–93.

Ataç, T. and A. Özgüç 1996. North-South Asymmetry in the Solar Flare Index, *Solar Physics,* 166, pp. 201–208.

Badalyan, O. G. and V. N. Obridko 2011. North-South Asymmetry of the Sunspot Indices and Its Quasi-Biennial Oscillations, *New Astronomy*, 16(6), pp. 357–365.

Ballester, J. L., R. Oliver, and M. Carbonell 2005. The Periodic Behaviour of the North-South Asymmetry of Sunspot Areas Revisited, *Astronomy and Astrophysics*, 431, pp. L5–L8.

Carbonell, M., R. Oliver and J. L. Ballester 1993. On the Asymmetry of Solar Activity, *Astronomy and Astrophysics*, 274, pp. 497–504.

Chang, H.-Y. 2007. Variation in North-South Asymmetry of Sun Spot Area, *Journal of Astronomy and Space Science*, 24(2), pp. 091–098.

Chang, H.-Y. 2008. Stochastic Properties in North-South Asymmetry of Sunspot Area, *New Astronomy*, 13(4), pp. 195–201.

Chowdhury, P., D. P. Choudhary, and S. Gosain 2013. A Study of the Hemispheric Asymmetry of Sunspot Area during Solar Cycles 23 and 24, *The Astrophysical Journal*, 768(2), pp. 188–198.

Donner, R. and M. Thiel 2007. Scale-Resolved Phase Coherence Analysis of Hemispheric Sunspot Activity: A New Look at the North-South Asymmetry, *Astronomy and Astrophysics*, 475(3), pp. L33–L36.

Duchlev, P. I. and V. N. Dermendjiev 1996. Periodicities in the N-S Asymmetry of Long-Lived Solar Filaments, Solar Physics, 168, pp. 205–210.

Garcia, H. A. 1990. Evidence for Solar-Cycle Evolution of North-South Flare Asymmetry during Cycles 20 and 21, *Solar Physics*, 127, pp. 185–197.

Joshi, B. and A. Joshi 2004. The North-South Asymmetry of Soft X-Ray Flare Index during Solar Cycles 21, 22 and 23, *Solar Physics*, 219, pp. 343–356.

Kiepenheuer, K. O. 1953. Chapter 6. Solar Activity, *The Sun*, G. P. Kuiper (ed.), *The Solar System*, Vol. I, The Univ. Chicago Press, Chicago, IL, pp. 322–465.

Knaack, R., J. O. Stenflo, and S. V. Berdyugina 2004. Periodic Oscillations in the North-South Asymmetry of the Solar Magnetic Field, *Astronomy and Astrophysics*, 418, pp. Ll7–L20.

Li, K. J. 2009. Systematic Time Delay of Hemispheric Solar Activity, *Solar Physics*, 255, pp. 169–177.

Li, K. J., J. X. Wang, S; Y. Xiong, H. F. Liang, H. S. Yun and X. M. Gu 2002. Regularity of the North-South Asymmetry of Solar Activity, *Astronomy and Astrophysics*, 383, pp. 648–652.

Li, K. J., H. D. Chen, L. S. Zhan, Q. X. Li, P. X. Gao, J. Mu, X. J. Shi and W. W. Zhu 2009. Asymmetry of Solar Activity in Cycle 23, *Journal of Geophysical Research*, 114, 6 pp.

Li, K. J., P. X. Gao and L. S. Zhan 2008. The Long-Term Behavior of the North-South Asymmetry of Sunspot Activity, *Solar Physics*, 254(1), pp. 145–154.

Li, K. J., P. X. Gao, L. S. Zhan and X. J. Shi 2009. The Long-Term Hemispheric Sunspot Activity, *The Astrophysical Journal*, 691(1), pp. 75–82.

Maunder, E. W. 1922. The Sun and Sunspots, 1820-1920, *Monthly Notices of the Royal Astronomical Society*, 82, pp. 534–543.

Newcomb, S. 1901. On the Period of the Solar Spots, *The Astrophysical Journal*, 13(1), pp. 1–14.

Newton, H. W. and A. S. Milson 1955. Note on the Observed Differences in Spottedness of the Sun's Northern and Southern Hemispheres, *Monthly Notices of the Royal Astronomical Society*, 115, pp. 398–404.

Oliver, R. and J. L. Ballester 1994. The North-South Asymmetry of Sunspot Areas during Solar Cycle 22, *Solar Physics*, 152, pp. 481–485.

Roy, J.-R. 1977. The North-South Distribution of Major Solar Flare Events, Sunspot Magnetic Classes and Sunspot Areas (1955–1974), *Solar Physics*, 52, pp. 53–61.

Schlamminger, L. 1991. Hemispherical Asymmetries in Sunspot Areas and Auroral Frequencies, *Solar Physics*, 135, pp. 407–413.

Swinson, D. B., H. Koyama, and T. Saito 1986. Long-Term Variations in North-South Asymmetry of Solar Activity, *Solar Physics*, 106, pp. 35–42.

Temmer, M., A. Veronig, and A. Hanslmeler 2002. Hemispheric Sunspot Numbers R_n and R_s: Catalogue and N-S Asymmetry Analysis, *Astronomy and Astrophysics*, 390, pp. 707–715.

Temmer, M., J. Rybak, P. Bendik, A. Veronig, F. Vogler, W. Otruba, W. Potzi, and A. Hanslmeier 2006. Hemispheric Sunspot Numbers R_n and R_s from 1945-2004: Catalogue and N-S Asymmetry Analysis for Solar Cycles 18-23, *Astronomy and Astrophysics*, 447(2), pp. 735–743.

Vernova, E. S., K. Mursula, M. I. Tyasto, and D. G. Baranov 2002. A New Pattern for the North South Asymmetry of Sunspots, *Solar Physics*, 205, pp. 371–382.

Vernova, E. S., K. Mursula, M. I. Tyasto, and D. G. Baranov 2004. Long-Term Longitudinal Asymmetries in Sunspot Activity: Difference between the Ascending and Descending Phase of the Solar Cycle, *Solar Physics*, 221, pp. 151–165.

Vizoso, G. and J. L. Ballester 1987. North-South Asymmetry in Sudden Disappearances of Solar Prominences, *Solar Physics*, 112, pp. 317–323.

Vizoso, G. and J. L. Ballester 1990. The North-South Asymmetry of Sunspot, *Astronomy and Astrophysics*, 229, pp. 540–546.

Waldmeier, M. 1971. The Asymmetry of Solar Activity in the Years 1959-1969, *Solar Physics*, 20, pp. 332–344.

Watari, S. 1996. Chaotic Behavior of the North-South Asymmetry of Sunspots? *Solar Physics*, 163, pp. 259–266.

Wilson R. M. 2019a. Predicting the Size and Timing of the Next Solar Cycle: Paper I, based on Sunspot Number, *Journal of the Alabama Academy of Science*, 90(2), pp. 70–92.

Wilson R. M. 2019b. Predicting the Size and Timing of the Next Solar Cycle: Paper II, based on Geomagnetic Values, *Journal of the Alabama Academy of Science*, 90(2), pp. 93–109.

Wilson, R. M. 2020. An Examination of the Sunspot Areal Dataset, 1875–2017: Paper I, an Overview, *Journal of the Alabama Academy of Science*, in press.

Yi, W. 1992. The North-South Asymmetry of Sunspot Distribution, *Journal of the Royal Astronomical Society of Canada*, 86, pp. 89–98.

Zharkov, S., V. V. Zharkova and S. S. Ipson 2005. Statistical Properties of Sunspots in 1996-2004:

I. Detection, North-South Asymmetry and Area Distribution, *Solar Physics*, 228, pp. 377–397.

Zolotova, N. V. and D. I. Ponyavin 2006. Phase Asynchrony ofthe North-South Sunspot Activity, *Astronomy and Astrophysics*, 449, pp. Ll–L4.

Zolotova, N. V. and D. I. Ponyavin 2007. Synchronization in Sunspot Indices in the Two Hemispheres, *Solar Physics*, 243, pp. l93–203.

Zolotova, N. V., D. I. Ponyavin, N. Marwan, and J. Kurths 2009. Long-Term Asymmetry in the Wings of the Butterfly Diagram, *Astronomy and Astrophysics*, 503, pp. 197–201.

MINUTES OF THE
ALABAMA ACADEMY OF SCIENCE
Executive Committee Meeting
Held via Zoom 10/23/2021 9:00 AM CST

Meeting was called to order at 9:10 am by Jack Shelley-Tremblay
Those in attendance were:

Prakash Sharma
Jack Shelley-Tremblay
Ellen Buckner
Cameron Gren
Mark Jones
Vinoy Thomas
Jonghwa Oh
Adriane Ludwick
Daniel Lerew
Jeff Morris
Ken Marion
David Nelson
Akshaya Kumar
Melvin Blake
Nisheeth Agrawal
Audrey Vasuaskas
Nancy Croomes
Jeff Morris

The meeting began with an introduction of the officers of the AAS.

The following is an update of the Action Items from the Spring Executive Committee meeting was done.

Action Item	**Person Responsible**	**Report**
Plans for 99th Annual Meeting, March 16-18, 2022	Athens State University Local Arrangements: Rick Roberts, co-Chair; Nick Agrawal, co-Chair; Nancy Croomes	Nancy Croomes and Nisheeth Agrawal provided a full update on the catering arrangements, technology set up, website arrangements, hotel arrangements, the keynote speaker, and the judging of student research competitions. All arrangements are in readiness, and Jack Shelley-Tremblay will provide web services through the academy website. Classrooms have a desktop that presenters can be used for their presentations, or presenters may bring laptops. A discussion of the fee structure determined that early registration deadlines are March 9, and that costs will be under budget. Everyone is encouraged to support early registration to by colleagues to support favorable pricing by catering. The title and abstract submission deadline is Feb 15. Membership confers a deep discount on the meeting fees, because the annual meeting is an outreach effort by the Academy. Jack Shelley-Tremblay moved to approve the fee structure and registration form. Matthew Edwards seconded. The motion passed.

		Ellen Buckner requested an update on COVID-19 precautions, and Nancy Croomes will share the protocols. Guidelines by the CDC will likely change by the time of the meeting. Ellen suggested that a pop-up clinic be available at the clinic and advocated for mask requirements. The Junior Academy and Gorgas may provide face shields, according to Ellen. Jack Shelley-Tremblay moved to include a statement in the meeting booklet that all attendees at the annual meeting are encouraged to get vaccinated and required to wear masks. Mark Jones expressed concern that NSTA does not allow students who aren't vaccinated to compete. This means that finalists that will proceed to nationals need to be notified in advance that they will need to be fully vaccinated in order to participate in the national competition. Discussion referenced flexibility and the potential of changing CDC recommendations. Nisheeth Agrawal expressed concerns that Athens State may have reservations about hosting a pop-up clinic. Since the AAS does not receive funds from the state of Alabama, they are likely not bound by restrictions on vaccine requirements at the state level. The motion passed. Ellen Buckner asked if digital posters might be possible. Classrooms have large displays, but not enough for each presenter to have one.
Identify Institutional Liaisons	Membership & Development	Cameron Gren presented on his efforts to contact deans about delegating

	Committee, Cameron Gren (Chair)	institutional Liaisons to encourage AAS membership and participation. Very few people responded. Ellen Buckner suggested that we reach out to all department chairs to invite them to join the AAS.
Approval of Trustee Nomination	Vinoy Thomas, Second Vice-President	Virginia Vilardi was nominated by Vinoy Thomas to fill Trustee vacancy (2021-24). Jack Shelley-Tremblay seconded the nomination. The motion passed.
AJAS and Gorgas competitions going forward	Task Force: Ellen Buckner, Mark Jones, Virginia Vilardi, Mary Lou Ewald, Mel Blake	Ellen Buckner, Mark Jones, and Mel Blake presented goals about developing the Alabama Science Trail for this budget year, and has funding for that project. Ellen requested volunteers to co-chair the effort. The difficulty of participation by rural students was discussed, and the problems associated with limited internet bandwidth. A movement for purchasing and providing hotspots for $1000 was proposed by Ellen Buckner. Jack Shelley-Tremblay amended the movement to request a quote and a discussion with Ken Marion and the budget committee to determine the feasibility. The movement passed.
Gorgas Scholarship Program Investment Account	Ken Marion, Chair, Budget and Finance	Ken Marion presented the report on Periodic Review of Gorgas Investment Account and the transition from the Alabama Power Foundation funding to private investment. Jim Sumpter is managing the investment account, with the goal of growing by 5 percent annually. Jack Shelley-Tremblay moved to schedule a subcommittee meeting (membership and development

		committee and Gorgas) to discuss developing corporate and private donors to enhance this fund.
Registration form 2022 meeting, Call for Papers	Larry Krannich	The call for papers announcement was examined. Jack Shelley-Tremblay moved to accept the document as presented. The motion passed.

Action Items for Spring 2022 meeting:

President Shelley-Tremblay then proceeded to go through the Committee reports. The minutes reflect the report discussions that occurred.

B-4:Vinoy Thomas is seeking a nomination for Archivist.

B-6: The detailed Treasury report is delayed because both of our banks have undergone a change in ownership. They closed one of the CDs and transferred roughly $18000 to the Alabama unclaimed property division. Bettina contacted the state and can retrieve the funds after Nov 1 2021. The other bank changed all account numbers and access passwords. Bettina will be going to the bank to access the new accounts.

B-9: Jack Shelley-Tremblay presented an update on the Science Fair. The AAS is hosting the state science fair this year, and he is working to enhance participation statewide and make student participation easier.

Jack Shelley-Tremblay offered a tribute to the long service of Larry Krannich as Executive Director of AAS. There will be a discussion of the transition to a new ED at the Spring 2022 meeting.

B-10: The science fair gave out a lot of awards and acquired a lot of new and renewed sponsors last year. Please view the website for details.

B-11: Science Olympiad needs a southern region host.

B-12: Matthew Edwards will be contacting Physics and Math chairs regionally, including Tennessee, in order to seek increased participation.

C-12: Dr Sharma discussed the AAS Awards and their requirements.

The meeting was adjourned at 11:15 AM.

Item	Responsible Persons	Issue
Development and Long Range Planning and Gorgas Committees develop donors for Gorgas Fund	Development and Long Range Planning and Gorgas Committees	These committees will have a joint meeting to discuss the development of corporate and private donors to grow the Gorgas fund.
Transition to new Executive Director and recognition of the long and excellent service by Larry Krannich	Jack Shelley-Tremblay	Discussion of the transition to a new ED.
Plan celebrations for the 100th anniversary of the AAS	Jack Shelley-Tremblay, Melvin Blake, Ellen Buckner	Discuss forming a committee for the 100th anniversary committee
Treasury Report	Bettina Riley	Update report on new bank accounts and retrieval of funds from the state of Alabama

Alabama Academy of Science Journal

Scope of the Journal:

The Alabama Academy of Science publishes significant, innovative research of interest to a wide audience of scientists in all areas. Papers should have a broad appeal, and particularly welcome will be studies that break new ground or advance our scientific understanding.

Information for the Authors:

- Manuscript layout should follow the specific guidelines of the journal.
- The authors are encouraged to contact the editor (E-mail: brtoone@samford.edu) prior to paper submission to obtain the guidelines for the author.
- At least one author must be a member of the *Alabama Academy of Science* (except for Special Papers).
- The author(s) should provide the names and addresses of at least two potential reviewers.
- Assemble the manuscript in the following order: Title Page, Abstract Page, Text, Brief acknowledgments (if needed), Literature Cited, Figure Legends, Tables, Figures.

Review Procedure and Policy:

Manuscripts will be reviewed by experts in the research area. Manuscripts receiving favorable reviews will be tentatively accepted. Copies of the reviewers' comments (and reviewer-annotated files of the manuscript, if any) will be returned to the correspondent author for any necessary revisions. The final revision and electronic copy are then submitted to the *Alabama Academy of Science Journal* Editor. The author is required to pay $100 for partial coverage of printing costs of the article.